Modelling Immune Dynamics in Locally Advanced MSI-H/dMMR Colorectal Cancer with Neoadjuvant Pembrolizumab Treatment: From Differential Equations to an Agent-Based Framework

Georgio Hawi[1, *], Peter Kim[1, †], and Peter P. Lee[2, †]

[1]School of Mathematics and Statistics, University of Sydney, Sydney, Australia
[2]Department of Immuno-Oncology, Beckman Research Institute, City of Hope, Duarte, California, USA
[*]Corresponding author: georgio.hawi@sydney.edu.au
[†]These authors contributed equally to this work

Abstract

Colorectal cancer (CRC) is the third most common malignancy worldwide, and accounts for approximately 10% of all cancers and an estimated 850,000 deaths annually. Within CRC, MSI-H/dMMR tumours are highly immunogenic due to their high mutational burden and neoantigen load, yet can evade immunosurveillance via PD-1/PD-L1-mediated signalling. Pembrolizumab, an anti-PD-1 antibody approved for unresectable or metastatic MSI-H/dMMR CRC, is emerging as a promising neoadjuvant option in the locally advanced setting, inducing rapid, deep and durable immune responses. In this work, we construct a minimal model of neoadjuvant pembrolizumab therapy in locally advanced MSI-H/dMMR CRC (laMCRC) using ordinary differential equations (ODEs), providing a highly extensible model that captures the main immune dynamics involved. On the other hand, agent-based models (ABMs) naturally capture stochasticity, interactions at an individual level, and discrete events that lie beyond the scope of differential-equation formulations. As such, we also convert our ODE model, with parameters calibrated to experimental data, to an ABM, preserving its dynamics while providing a flexible platform for future mechanistic investigation and modelling.

Keywords: locally advanced MSI-H/dMMR colorectal cancer, pembrolizumab, ordinary differential equations, agent-based modelling, minimal model

1 Introduction

Colorectal cancer (CRC)—the world's third most common malignancy, accounting for approximately 10% of all cancers [1] and more than 1.85 million cases with 850,000 deaths annually [2]—remains a major burden, with the American Cancer Society projecting 154,270 new CRC diagnoses and 52,900 deaths in the United States due to CRC in 2025 [3]. A key phenotype within CRC is that of microsatellite instability–high/mismatch repair–deficient (MSI-H/dMMR) disease, characterised by a highly immunogenic tumour microenvironment (TME) driven by markedly elevated somatic mutation

rates, tumour mutational burden (TMB), and neoantigen load [4–6]. Although approximately 20% of stage II and 12% of stage III CRC tumours are MSI-H/dMMR [7, 8], patients with this hypermutant phenotype respond poorly to conventional 5-fluorouracil–based chemotherapy [9, 10] yet show striking responsiveness to immune checkpoint inhibitors (ICIs) [11].

Immune checkpoints, such as programmed cell death-1 (PD-1), a cell membrane receptor that is expressed on a variety of cell types, including activated T cells, activated NK cells and monocytes, normally downregulate immune responses after antigen activation [12]. PD-1 has been extensively studied in cancer, including MSI-H/dMMR CRC [13, 14]; engagement by its ligands PD-L1 and PD-L2 inhibits effector T-cell activity, suppresses pro-inflammatory cytokine secretion, and promotes expansion of regulatory T cells (Tregs) [15, 16]. Tumours further exploit this pathway by expressing PD-L1 themselves, thereby impairing cytotoxic T-lymphocyte (CTL) and natural killer (NK) cell activity [17]. However, blocking PD-1/PD-L1 complex formation reinvigorates effector T cells, enhances anti-tumour immunity, and improves clinical outcomes [18, 19]. Pembrolizumab, a fully human IgG4 anti–PD-1 antibody, demonstrated significant efficacy in metastatic MSI-H/dMMR CRC in the phase III KEYNOTE-177 trial (NCT02563002) [20], leading the FDA to approve pembrolizumab for first-line treatment of unresectable or metastatic MSI-H/dMMR CRC on June 29, 2020 [21].

Furthermore, in recent years, interest in neoadjuvant pembrolizumab for the treatment of high-risk stage II and stage III MSI-H/dMMR CRC has surged [22]. In the phase II NEOPRISM-CRC study (NCT05197322), 31 patients with high TMB and high-risk stage II–III MSI-H/dMMR CRC received three cycles of pembrolizumab followed by surgery 4–6 weeks later; pathologic complete response (pCR) was achieved in 17 patients, and no recurrences were observed at a median 6-month follow-up [23]. Another phase II trial, NCT04082572, evaluated the efficacy of neoadjuvant pembrolizumab in localised MSI-H/dMMR solid tumours [24]. In the locally advanced MSI-H/dMMR CRC (laMCRC) cohort, 27 patients received pembrolizumab 200 mg IV every 3 weeks either for up to 16 cycles or eight cycles followed by resection. Overall, 21 patients exhibited pCR, and among the 14 patients in the resection group, 11 achieved pCRs. At a median 9.5-month follow-up, only two recurrences/progressions were observed, and at a median 3-year follow-up, no late progression events occurred, demonstrating the efficacious and durable response of pembrolizumab in localised dMMR/MSI-H tumours [25].

Mathematical models provide a powerful framework for analysing the immunobiology underpinning diseases, and, when mechanistic, for investigating the dynamics of key biological components to improve theoretical understanding. They also enable the optimisation of treatment regimens whilst avoiding the substantial time and financial costs of human clinical trials. Numerous immunobiological models of CRC exist [26–29], and ICI therapy has been modelled extensively in other cancers [30–34]. Nonetheless, there are a multitude of limitations and drawbacks to these models of CRC and ICI therapy, as detailed in [35]. In this work, we focus on our comprehensive model of neoadjuvant pembrolizumab therapy in laMCRC [35], which, to the authors' knowledge, is the only deterministic immunobiological model of ICI therapy in CRC and addresses many of these drawbacks.

However, to effectively model complex biological systems, one must master the balance between model complexity and model accuracy. Traditional mechanistic models often incorporate many processes, leading to numerous state variables, inputs, and parameters [36]. As such, it is ideal to reduce models such that their key dynamics are preserved, while pruning parameters and inputs with minimal influence on the outputs. The full model in [35] is large, comprising complex delay integro-differential equations with many components and interactions. In this work, we construct a minimal model of pembrolizumab therapy in laMCRC using ordinary differential equations (ODEs), avoiding these

complexities, to reveal the core immune dynamics and interactions, and accurately replicate the state-variable trajectories of the full model.

Agent-based models (ABMs) are well-suited to model complex biological systems, such as cancer, due to their ability to explicitly represent individual entities and their interactions, incorporate spatial structure, and capture phenotypic heterogeneity [37, 38]. Their inherent stochasticity enables the estimation of probabilities and predictive intervals for treatment response—features which are impossible to be predicted by differential equations due to their deterministic, mean-field nature [39]. As such, ABMs are being increasingly used to model cancer dynamics, with Kather et al. developing patient-informed ABMs have been used to study the response of combined immunotherapy and stroma-targeting therapies in CRC [40], as well as enable in-silico screening of combination immunotherapies [41]. For ICIs broadly, multiscale ABMs of PD-1/PD-L1 interactions have reproduced spatiotemporal tumour-CTL dynamics and linked response to ICIs to antigenicity and TMB [42].

Nonetheless, because ABMs typically encode many interactions and processes, their stochastic and computationally expensive simulations make statistical calibration of model parameters to experimental data difficult. In this work, we outline a practical workflow for converting ODE models to ABMs and apply this to our minimal ODE model of neoadjuvant pembrolizumab therapy in laMCRC, allowing for accurate and efficient parameter estimation of the ABM. We finally compare ABM trajectories of model components with those from the minimal ODE model and the full model from [35], verifying consistency and faithful reproduction of all dynamics, thereby laying a foundation for future ABMs of laMCRC and other cancers.

2 A Minimal Model of Locally Advanced MSI-H/dMMR CRC

The derivation of many equations in the minimal model closely follows [35], but is repeated here for the sake of completeness.

2.1 Model Variables

The variables and their units in the minimal model are shown in Table 1.

2.2 Model Diagrams

Diagrams encompassing the interactions of model components in the TS and TDLN are shown in Figure 1 and Figure 2, respectively.

2.3 Model Assumptions

For simplicity, we ignore spatial effects in the model, ignoring the effects of diffusion, advection, and chemotaxis by all species. We assume the system has one compartment, being the TS, located in the colon or rectum. This is a simplification since locally advanced CRC typically involves multiple tumour-draining lymph nodes [43]; however, for simplicity, we focus on the sentinel node and refer to it as the TDLN for the purposes of the model. We assume that cytokines in the TS are produced only by effector or activated cells and that DAMPs in the TS are only produced by necrotic cancer cells. We assume that all mature DCs considered in the TDLN are cancer-antigen-bearing and that all T cells considered in the TS are primed with cancer antigens. Furthermore, we assume that all activated T

Var	Description	Var	Description
C	Viable cancer cell density	N_c	Necrotic cell density
D_0	Immature DC density	D	Mature DC density in the TS
D^{LN}	Mature DC density in the TDLN	T_0^8	Naive CD8+ T cell density in the TDLN
T_A^8	Effector CD8+ T cell density in the TDLN	T_8	Effector CD8+ T cell density in the TS
T_{ex}	Exhausted CD8+ T cell density in the TS	T_0^r	Naive Treg density in the TDLN
T_A^r	Effector Treg density in the TDLN	T_r	Effector Treg density in the TS
M_0	Naive macrophage density	M_2	M2 macrophage density
K_0	Resting NK cell density	K	Activated NK cell density
I_2	IL-2 concentration	I_γ	IFN-γ concentration
I_α	TNF concentration	I_β	TGF-β concentration
I_{10}	IL-10 concentration	I_{12}	IL-12 concentration
$P_D^{T_8}$	Unbound PD-1 receptor concentration on effector CD8+ T cells in the TS	P_D^K	Unbound PD-1 receptor concentration on activated NK cells
$Q_A^{T_8}$	PD-1/pembrolizumab complex concentration on effector CD8+ T cells in the TS	Q_A^K	PD-1/pembrolizumab complex concentration on activated NK cells
P_L	Unbound PD-L1 concentration in the TS	Q^{T_8}	PD-1/PD-L1 complex concentration on effector CD8+ T cells in the TS
Q^K	PD-1/PD-L1 complex concentration on activated NK cells	A_1	Concentration of pembrolizumab in the TS
$P_D^{8\mathrm{LN}}$	Unbound PD-1 receptor concentration on effector CD8+ T cells in the TDLN	$Q_A^{8\mathrm{LN}}$	PD-1/pembrolizumab complex concentration on effector CD8+ T cells in the TDLN
P_L^{LN}	Unbound PD-L1 concentration in the TDLN	$Q^{8\mathrm{LN}}$	PD-1/PD-L1 complex concentration on effector CD8+ T cells in the TDLN
A_1^{LN}	Concentration of pembrolizumab in the TDLN		

Table 1: Variables used in the model. Quantities in the top box are in units of cell/cm^3, quantities in the second box are in units of g/cm^3, and all other quantities are in units of molec/cm^3. All quantities pertain to the tumour site.

cells considered in the TDLN are activated with cancer antigens and that T cell proliferation/division follows a deterministic program. We ignore CD8+ memory T cells. We also assume that all Tregs are natural Tregs (nTregs), ignoring induced Tregs (iTregs). We also assume that the duration of pembrolizumab infusion is negligible compared to the timescale of the model. Therefore, we treat their infusions as an intravenous bolus so that drug absorption occurs immediately after infusion. Finally, we assume a constant solution history, where the history for each species is set to its respective initial condition.

We assume that all species, X_i, degrade/die at a rate proportional to their concentration, with decay constant d_{X_i}. We assume that the rate of activation/polarisation of a species X_i by a species X_j follows the Michaelis-Menten kinetic law $\lambda_{X_iX_j} X_i \frac{X_j}{K_{X_iX_j}+X_j}$, for rate constant $\lambda_{X_iX_j}$, and half-saturation constant $K_{X_iX_j}$. Similarly, we model the rate of inhibition of a species X_i by a species X_j using a term with form $\lambda_{X_iX_j} \frac{X_i}{1+X_j/K_{X_iX_j}}$ for rate constant $\lambda_{X_iX_j}$, and inhibition constant $K_{X_iX_j}$. Production of X_i by X_j is modelled using mass-action kinetics unless otherwise specified, so that the rate at which X_i is formed is given by $\lambda_{X_iX_j} X_j$ for some positive constant $\lambda_{X_iX_j}$. Finally, we assume that the rate of lysis of X_i by X_j follows mass-action kinetics in the case where X_j is a cell and follows Michaelis-Menten

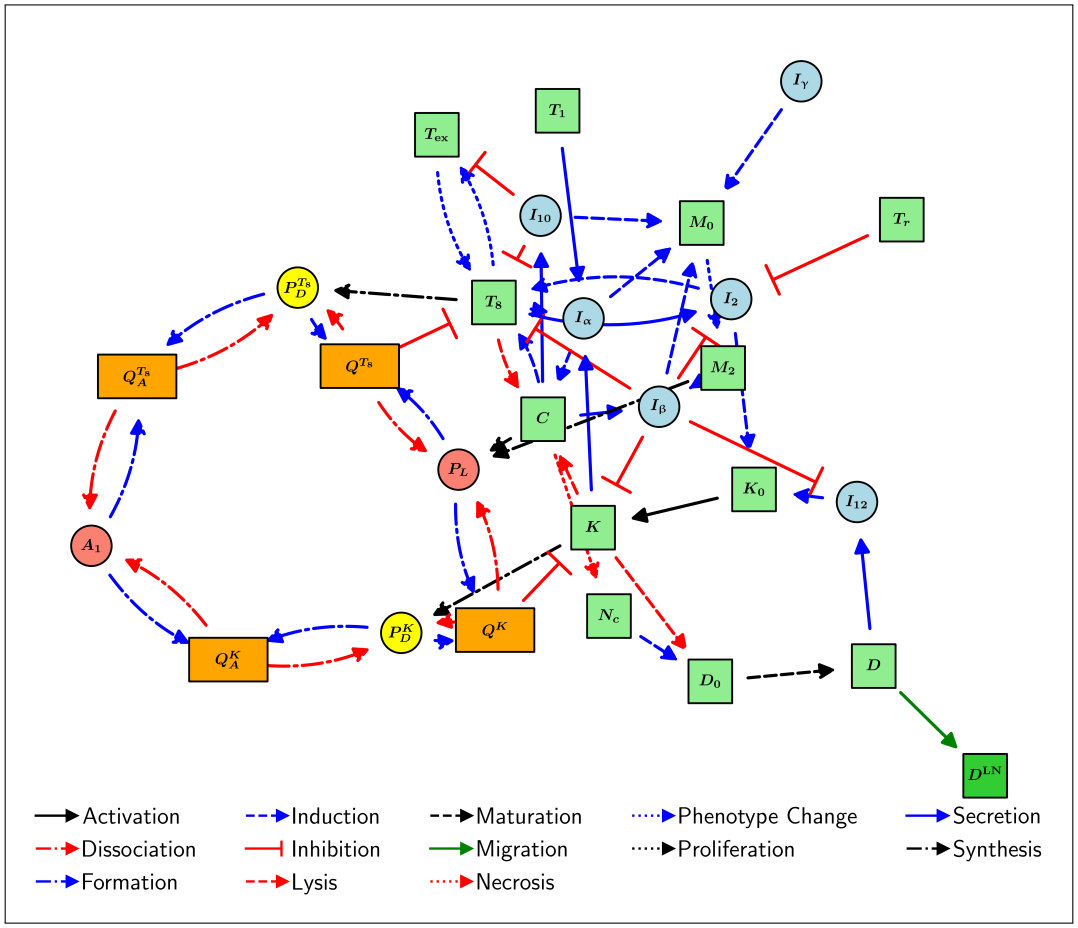

Figure 1: Schematic diagram of the interactions of model components in the TS.

kinetics in the case where X_j is a cytokine.

2.4 Model Equations

2.4.1 Equations for Cancer Cells (C and N_c)

Viable cancer cells are killed by effector CD8+ T cells [44] and activated NK cells [45] through direct contact, whilst TNF indirectly eliminates cancer cells via activating cell death pathways [46–48]. In particular, TNF induces the necroptosis, programmed necrotic cell death, of cancer cells [47, 49]. We note that TGF-β and the PD-1/PD-L1 complex inhibit cancer cell lysis by CD8+ T cells [50–52], and that TGF-β and PD-1/PD-L1 have been shown to inhibit NK cell cytotoxicity [15, 53–57]. We assume that viable cancer cells grow logistically, as is done in many CRC models [26, 27, 29], due to space and resource competition in the TME. Combining these, we have

$$\frac{dC}{dt} = \underbrace{\lambda_C C\left(1-\frac{C}{C_0}\right)}_{\text{growth}} - \underbrace{\lambda_{CT_8} T_8 \frac{1}{1+I_\beta/K_{CI_\beta}} \frac{1}{1+Q^{T_8}/K_{CQ^{T_8}}} C}_{\substack{\text{elimination by } T_8 \\ \text{inhibited by } I_\beta \text{ and } Q^{T_8}}} - \underbrace{\lambda_{CK} K \frac{1}{1+I_\beta/K_{CI_\beta}} \frac{1}{1+Q^K/K_{CQ^K}} C}_{\substack{\text{elimination by } K \\ \text{inhibited by } I_\beta \text{ and } Q^K}}$$

$$- \underbrace{\lambda_{CI_\alpha} \frac{I_\alpha}{K_{CI_\alpha}+I_\alpha} C}_{\text{elimination by } I_\alpha}, \tag{2.1}$$

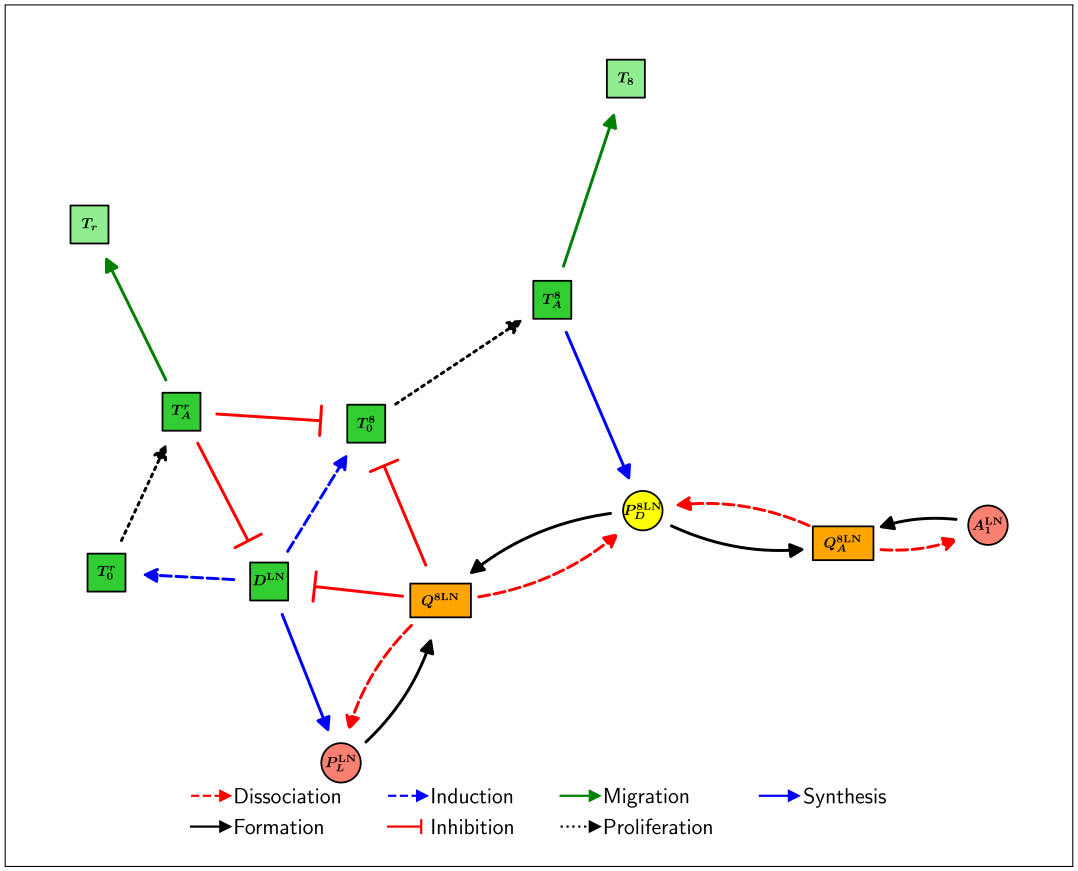

Figure 2: Schematic diagram of the interactions of model components in the TDLN.

$$\frac{dN_c}{dt} = \underbrace{\lambda_{CI_\alpha} \frac{I_\alpha}{K_{CI_\alpha} + I_\alpha} C}_{\text{elimination by } I_\alpha} - \underbrace{d_{N_c} N_c}_{\text{removal}}. \tag{2.2}$$

2.4.2 Equations for Immature and Mature DCs in the TS (D_0 and D)

Immature DCs are stimulated to mature via DAMPs, such as HMGB1 [58], whose concentration is assumed to be proportional to that of necrotic cancer cells. In addition, activated NK cells have been shown to efficiently kill immature DCs but not mature DCs; however, this is inhibited by TGF-β [59–61]. We also need to consider that some mature DCs migrate into the T cell zone of the TDLN and stimulate naive T cells, causing them to be activated [62, 63]. Assuming that immature DCs are supplied at a rate $\mathcal{A}_{D_0}$, we have that

$$\frac{dD_0}{dt} = \underbrace{\mathcal{A}_{D_0}}_{\text{source}} - \underbrace{\lambda_{DN_c} D_0 \frac{N_c}{K_{DN_c} + N_c}}_{D_0 \to D \text{ by } N_c} - \underbrace{\lambda_{D_0 K} D_0 K \frac{1}{1 + I_\beta / K_{D_0 I_\beta}}}_{\substack{\text{elimination by } K \\ \text{inhibited by } I_\beta}} - \underbrace{d_{D_0} D_0}_{\text{death}}, \tag{2.3}$$

$$\frac{dD}{dt} = \underbrace{\lambda_{DN_c} D_0 \frac{N_c}{K_{DN_c} + N_c}}_{D_0 \to D \text{ by } N_c} - \underbrace{\lambda_{DD^{\text{LN}}} D}_{\substack{D \text{ migration} \\ \text{to TDLN}}} - \underbrace{d_D D}_{\text{death}}. \tag{2.4}$$

2.4.3 Equation for Mature DCs in the TDLN (D^{LN})

We assume a fixed DC migration time of τ_m and also assume that only $\exp(-d_D\tau_m)$ of the mature DCs that leave the TS survive migration. We also assume that the concentration of mature DCs in the TDLN does not change significantly during migration. Taking into account the volume change between the TS and the TDLN, we have that

$$\frac{dD^{\mathrm{LN}}}{dt} = \frac{V_{\mathrm{TS}}}{V_{\mathrm{LN}}} \underbrace{\lambda_{DD^{\mathrm{LN}}} \exp(-d_D\tau_m)\, D}_{D \text{ migration to TDLN}} - \underbrace{d_D D^{\mathrm{LN}}}_{\text{death}}. \tag{2.5}$$

2.4.4 Equation for Naive CD8+ T Cells in the TDLN (T_0^8)

We assume that naive CD8+ T cells come into the TDLN at a constant rate and that they have not undergone cell division, nor will they until their activation, which we assume to occur instantaneously. For simplicity, we do not consider cytokines in the TDLN, absorbing their influence into $\lambda_{T_0^8 T_A^8}$. We do, however, explicitly take into account the influence of effector Tregs and the PD-1/PD-L1 complex in the TDLN, which have been shown to inhibit T cell activation via mechanisms including limiting naive T cells from binding to mature DCs [64–72]. Recalling that T cells that have become activated by mature DCs are no longer naive, and taking this all into account, leads to

$$\frac{dT_0^8}{dt} = \underbrace{\mathcal{A}_{T_0^8}}_{\text{source}} - \underbrace{\lambda_{T_0^8 T_A^8} R^8}_{\substack{\text{CD8+ T cell}\\ \text{activation}}} - \underbrace{d_{T_0^8} T_0^8}_{\text{death}}, \tag{2.6}$$

where R^8 is defined as

$$R^8 := \underbrace{\frac{D^{\mathrm{LN}} T_0^8}{\left(1 + T_A^r / K_{T_0^8 T_A^r}\right)\left(1 + Q^{8\mathrm{LN}} / K_{T_0^8 Q^{8\mathrm{LN}}}\right)}}_{\text{CD8+ T cell activation inhibited by } T_A^r \text{ and } Q^{8\mathrm{LN}}}. \tag{2.7}$$

2.4.5 Equation for Effector CD8+ T Cells in the TDLN (T_A^8)

It is known that activated CD8+ T cells undergo clonal expansion in the TDLN and differentiate before they stop proliferating and migrate to the TS [73, 74].

We assume that activated CD8+ T cells proliferate up to $n^8_{\max}$ times, upon which they stop dividing. For simplicity, we assume that the death rate of CD8+ T cells that have not completed their division program is equal to $d_{T_0^8}$, the death rate of naive CD8+ T cells, regardless of the number of cell divisions previously undergone. We also assume that only activated CD8+ T cells that have undergone $n^8_{\max}$ divisions become effector CD8+ T cells, which will leave the TDLN and migrate to the TS. Furthermore, we assume a constant cell cycle time of Δ_8, except for the first cell division, which has a cycle time of Δ_8^0. Thus, the duration of the activated CD8+ T cell division program to $n^8_{\max}$ divisions is given by

$$\tau_{T_A^8} := \Delta_8^0 + (n^8_{\max} - 1)\Delta_8. \tag{2.8}$$

In particular, we must take into account that some T cells will die before the division program is complete, so we must introduce a shrinkage factor of $\exp\left(-d_{T_0^8}\tau_{T_A^8}\right)$. Additionally, we assume that the concentration of components in the TDLN does not change significantly during proliferation. Furthermore, we must also take into account that effector Tregs and the PD-1/PD-L1 complex inhibit

CD8+ T cell proliferation throughout the program [65–67, 75, 76]. We must also consider that some of these effector CD8+ T cells will migrate to the TS to perform effector functions. We finally assume that the death rate of CD8+ T cells that have completed their division program is equal to the death rate of CD8+ T cells in the TS. Taking this all into account leads to

$$\frac{dT_A^8}{dt} = \underbrace{\frac{2^{n_{\max}^8} \exp\left(-d_{T_0^8}\tau_{T_A^8}\right)\lambda_{T_0^8 T_A^8} R^8}{\left(1 + T_A^r/K_{T_A^8 T_A^r}\right)\left(1 + Q^{8\mathrm{LN}}/K_{T_A^8 Q^{8\mathrm{LN}}}\right)}}_{\text{CD8+ T cell proliferation inhibited by } T_A^r \text{ and } Q^{8\mathrm{LN}}} - \underbrace{\lambda_{T_A^8 T_8} T_A^8}_{\substack{T_A^8 \text{ migration} \\ \text{to the TS}}} - \underbrace{d_{T_8} T_A^8}_{\text{death}}. \tag{2.9}$$

2.4.6 Equations for Effector and Exhausted CD8+ T Cells in the TS (T_8 and T_{ex})

We assume that it takes τ_a amount of time for effector CD8+ T cells in the TDLN to migrate to the TS. Like with DCs, we assume that the concentration of effector CD8+ T cells in the TDLN does not change significantly during migration. We must also account for CTL expansion due to IL-2 [77], noting that this proliferation is inhibited by effector Tregs [65–67]. Furthermore, the death of CD8+ T cells is resisted by IL-10 [78, 79].

However, chronic antigen exposure can cause effector CD8+ T cells to enter a state of exhaustion, where they lose their ability to kill cancer cells, and the rate of cytokine secretion significantly decreases [80–82]. We denote this exhausted CD8+ T cell population as T_{ex}. It has also been shown that pembrolizumab can "reinvigorate" these cells back into the effector state [18, 83]. We model the re-invigoration and exhaustion using Michaelis-Menten terms in A_1 and C, respectively. In particular, this has been shown to be more appropriate than simple mass-action kinetics as it accounts for extended antigen exposure [84].

As such, remembering to take the volume change between the TDLN and the TS into account, this implies that

$$\begin{aligned}\frac{dT_8}{dt} = \frac{V_{\mathrm{LN}}}{V_{\mathrm{TS}}} &\underbrace{\lambda_{T_A^8 T_8} \exp\left(-d_{T_8}\tau_a\right) T_A^8}_{T_A^8 \text{ migration to the TS}} + \underbrace{\lambda_{T_8 I_2} \frac{T_8 I_2}{K_{T_8 I_2} + I_2} \frac{1}{1 + T_r/K_{T_8 T_r}}}_{\text{growth by } I_2 \text{ inhibited by } T_r} \\ &- \underbrace{\lambda_{T_8 C} \frac{T_8 C}{K_{T_8 C} + C}}_{T_8 \to T_{\mathrm{ex}} \text{ from } C \text{ exposure}} + \underbrace{\lambda_{T_{\mathrm{ex}} A_1} \frac{T_{\mathrm{ex}} A_1}{K_{T_{\mathrm{ex}} A_1} + A_1}}_{T_{\mathrm{ex}} \to T_8 \text{ by } A_1} - \underbrace{\frac{d_{T_8} T_8}{1 + I_{10}/K_{T_8 I_{10}}}}_{\substack{\text{death} \\ \text{inhibited by } I_{10}}},\end{aligned} \tag{2.10}$$

$$\frac{dT_{\mathrm{ex}}}{dt} = \underbrace{\lambda_{T_8 C} \frac{T_8 C}{K_{T_8 C} + C}}_{T_8 \to T_{\mathrm{ex}} \text{ from } C \text{ exposure}} - \underbrace{\lambda_{T_{\mathrm{ex}} A_1} \frac{T_{\mathrm{ex}} A_1}{K_{T_{\mathrm{ex}} A_1} + A_1}}_{T_{\mathrm{ex}} \to T_8 \text{ by } A_1} - \underbrace{\frac{d_{T_{\mathrm{ex}}} T_{\mathrm{ex}}}{1 + I_{10}/K_{T_{\mathrm{ex}} I_{10}}}}_{\substack{\text{death} \\ \text{inhibited by } I_{10}}}. \tag{2.11}$$

2.4.7 Equation for Naive Tregs in the TDLN (T_0^r)

We also consider the concentration of naive Tregs in the TDLN, following the same procedure as for CD8+ T cells. We absorb the influence of cytokines on Treg activation via the kinetic rate constant $\lambda_{T_0^r T_A^r}$. We also take into account that some mature DCs migrate into the TDLN and activate naive Tregs, causing them to no longer be naive. Assuming that naive Tregs come into the TDLN at a rate

$\mathcal{A}_{T_0^r}$, we can write a similar equation to (2.6):

$$\frac{dT_0^r}{dt} = \underbrace{\mathcal{A}_{T_0^r}}_{\text{source}} - \underbrace{\lambda_{T_0^r T_A^r} R^r}_{\text{Treg activation}} - \underbrace{d_{T_0^r} T_0^r}_{\text{death}}, \tag{2.12}$$

where R^r is defined as

$$R^r := \underbrace{D^{\text{LN}} T_0^r}_{\text{Treg activation}} . \tag{2.13}$$

2.4.8 Equation for Effector Tregs in the TDLN (T_A^r)

We assume that activated Tregs proliferate up to $n_{\max}^r$ times, upon which they stop dividing and become effector Tregs. As before, we assume that the death rate of Tregs that have not completed their division program is equal to $d_{T_0^r}$, the death rate of naive Tregs. We assume a constant cell cycle time of Δ_r, except for the first cell division, which has a cycle time of Δ_r^0. Thus, the duration of the activated Treg division program to $n_{\max}^r$ divisions is given by

$$\tau_{T_A^r} := \Delta_r^0 + (n_{\max}^r - 1)\Delta_r. \tag{2.14}$$

In particular, we must take into account that some T cells will die before the division program is complete, so we must introduce a shrinkage factor of $\exp\left(-d_{T_0^r}\tau_{T_A^r}\right)$. We, again, assume that the concentration of components in the TDLN does not change significantly during proliferation. We also assume that the death rate of effector Tregs in the TDLN is equal to the corresponding degradation rate in the TS. Taking this all into account, and incorporating effector Treg migration to the TS, leads to

$$\frac{dT_A^r}{dt} = \underbrace{2^{n_{\max}^r} \exp\left(-d_{T_0^r}\tau_{T_A^r}\right) \lambda_{T_0^r T_A^r} R^r}_{\text{Treg proliferation}} - \underbrace{\lambda_{T_A^r T_r} T_A^r}_{\substack{T_A^r \text{ migration} \\ \text{to the TS}}} - \underbrace{d_{T_r} T_A^r}_{\text{death}}. \tag{2.15}$$

2.4.9 Equation for Effector Tregs in the TS (T_r)

Assuming that it also takes τ_a amount of time for Tregs to migrate to the TS, and that the concentration of effector Tregs in the TDLN does not change significantly during migration, we have that

$$\frac{dT_r}{dt} = \frac{V_{\text{LN}}}{V_{\text{TS}}} \underbrace{\lambda_{T_A^r T_r} \exp\left(-d_{T_r}\tau_a\right) T_A^r}_{T_A^r \text{ migration to the TS}} - \underbrace{d_{T_r} T_r}_{\text{death}}. \tag{2.16}$$

2.4.10 Equations for Naive and M2 Macrophages (M_0 and M_2)

While we only consider naive and anti-inflammatory M2 macrophages, we must also take into account that some naive macrophages polarise to the pro-inflammatory M1 phenotype, whose density we denote as M_1. In particular, IFN-γ and TNF polarise naive macrophages into M1 macrophages [85–88], whilst TGF-β and IL-10 polarise naive macrophages into the M2 phenotype [89–91]. Assuming a production

rate $\mathcal{A}_{M_0}$ of naive macrophages, we thus have that

$$\begin{aligned}\frac{dM_0}{dt} &= \underbrace{\mathcal{A}_{M_0}}_{\text{source}} - \underbrace{\lambda_{M_1 I_\gamma} M_0 \frac{I_\gamma}{K_{M_1 I_\gamma} + I_\gamma}}_{M_0 \to M_1 \text{ by } I_\gamma} - \underbrace{\lambda_{M_1 I_\alpha} M_0 \frac{I_\alpha}{K_{M_1 I_\alpha} + I_\alpha}}_{M_0 \to M_1 \text{ by } I_\alpha} - \underbrace{\lambda_{M_2 I_\beta} M_0 \frac{I_\beta}{K_{M_2 I_\beta} + I_\beta}}_{M_0 \to M_2 \text{ by } I_\beta} \\ &\quad - \underbrace{\lambda_{M_2 I_{10}} M_0 \frac{I_{10}}{K_{M_2 I_{10}} + I_{10}}}_{M_0 \to M_2 \text{ by } I_{10}} - \underbrace{d_{M_0} M_0}_{\text{degradation}} ,\end{aligned} \tag{2.17}$$

$$\frac{dM_2}{dt} = \underbrace{\lambda_{M_2 I_\beta} M_0 \frac{I_\beta}{K_{M_2 I_\beta} + I_\beta}}_{M_0 \to M_2 \text{ by } I_\beta} + \underbrace{\lambda_{M_2 I_{10}} M_0 \frac{I_{10}}{K_{M_2 I_{10}} + I_{10}}}_{M_0 \to M_2 \text{ by } I_{10}} - \underbrace{d_{M_2} M_2}_{\text{degradation}} . \tag{2.18}$$

2.4.11 Equations for Resting and Activated NK Cells (K_0 and K)

Resting NK cells are activated by IL-2 and IL-12 [92, 93]. However, NK cell activation is inhibited by TGF-β [94]. Thus, assuming a supply rate $\mathcal{A}_{K_0}$ of resting NK cells, we have that

$$\frac{dK_0}{dt} = \underbrace{\mathcal{A}_{K_0}}_{\text{source}} - \left(\underbrace{\lambda_{K I_2} K_0 \frac{I_2}{K_{K I_2} + I_2}}_{K_0 \to K \text{ by } I_2} + \underbrace{\lambda_{K I_{12}} K_0 \frac{I_{12}}{K_{K I_{12}} + I_{12}}}_{K_0 \to K \text{ by } I_{12}} \right) \underbrace{\frac{1}{1 + I_\beta / K_{K I_\beta}}}_{\substack{\text{activation} \\ \text{inhibited by } I_\beta}} - \underbrace{d_{K_0} K_0}_{\text{degradation}} , \tag{2.19}$$

$$\frac{dK}{dt} = \left(\underbrace{\lambda_{K I_2} K_0 \frac{I_2}{K_{K I_2} + I_2}}_{K_0 \to K \text{ by } I_2} + \underbrace{\lambda_{K I_{12}} K_0 \frac{I_{12}}{K_{K I_{12}} + I_{12}}}_{K_0 s \to K \text{ by } I_{12}} \right) \underbrace{\frac{1}{1 + I_\beta / K_{K I_\beta}}}_{\substack{\text{activation} \\ \text{inhibited by } I_\beta}} - \underbrace{d_K K}_{\text{degradation}} . \tag{2.20}$$

2.4.12 Equation for IL-2 (I_2)

IL-2 is produced by effector CD8+ T cells [95, 96], so that

$$\frac{dI_2}{dt} = \underbrace{\lambda_{I_2 T_8} T_8}_{\text{production by } T_8} - \underbrace{d_{I_2} I_2}_{\text{degradation}} . \tag{2.21}$$

2.4.13 Equation for IFN-γ (I_γ)

IFN-γ is produced by activated NK cells [97] so that

$$\frac{dI_\gamma}{dt} = \underbrace{\lambda_{I_\gamma K} K}_{\text{production by } K} - \underbrace{d_{I_\gamma} I_\gamma}_{\text{degradation}} . \tag{2.22}$$

2.4.14 Equation for TNF (I_α)

TNF is produced by effector CD8+ T cells [98, 99] and activated NK cells [100, 101]. Hence,

$$\frac{dI_\alpha}{dt} = \underbrace{\lambda_{I_\alpha T_8} T_8}_{\text{production by } T_8} + \underbrace{\lambda_{I_\alpha K} K}_{\text{production by } K} - \underbrace{d_{I_\alpha} I_\alpha}_{\text{degradation}} . \tag{2.23}$$

2.4.15 Equation for TGF-β (I_β)

TGF-β is produced by viable cancer cells [102] and M2 macrophages [90, 103]. Thus,

$$\frac{dI_\beta}{dt} = \underbrace{\lambda_{I_\beta C} C}_{\text{production by } C} + \underbrace{\lambda_{I_\beta M_2} M_2}_{\text{production by } M_2} - \underbrace{d_{I_\beta} I_\beta}_{\text{degradation}} . \tag{2.24}$$

2.4.16 Equation for IL-10 (I_{10})

IL-10 is produced by viable cancer cells [104, 105] so that

$$\frac{dI_{10}}{dt} = \underbrace{\lambda_{I_{10} C} C}_{\text{production by } C} - \underbrace{d_{I_{10}} I_{10}}_{\text{degradation}} . \tag{2.25}$$

2.4.17 Equation for IL-12 (I_{12})

IL-12 is produced by mature DCs [106] so that

$$\frac{dI_{12}}{dt} = \underbrace{\lambda_{I_{12} D} D}_{\text{production by } D} - \underbrace{d_{I_{12}} I_{12}}_{\text{degradation}} . \tag{2.26}$$

2.4.18 Equations for Unbound PD-1 receptors on Cells in the TS ($P_D^{T_8}$ and P_D^K)

It is known that PD-1 is expressed on the surface of effector CD8+ T cells [107–109] and activated NK cells [55, 57, 110]. We assume that the rate of PD-1 synthesis is proportional to the concentration of the cell expressing it. However, unbound PD-1 receptors on these PD-1-expressing cells can bind to either pembrolizumab or PD-L1, forming the PD-1/pembrolizumab and PD-1/PD-L1 complexes, respectively, resulting in the depletion of unbound PD-1 molecules [16, 111]. For simplicity, we assume that the formation and dissociation rates of the PD-1/PD-L1 and PD-1/pembrolizumab complexes are invariant of the type of cell expressing PD-1. Considering unbound PD-1 receptors on effector CD8+ T cells in the TS at first, and taking into account the degradation of PD-1 receptors, this motivates the equation for $P_D^{T_8}$ to be

$$\frac{dP_D^{T_8}}{dt} = \underbrace{\lambda_{P_D^{T_8}} T_8}_{\text{synthesis}} + \underbrace{\lambda_{Q_A} Q_A^{T_8}}_{\substack{\text{dissociation}\\ \text{of } Q_A^{T_8}}} + \underbrace{\lambda_Q Q^{T_8}}_{\substack{\text{dissociation}\\ \text{of } Q^{T_8}}} - \underbrace{\lambda_{P_D A_1} P_D^{T_8} A_1}_{\text{binding to } A_1} - \underbrace{\lambda_{P_D P_L} P_D^{T_8} P_L}_{\text{binding to } P_L} - \underbrace{d_{P_D} P_D^{T_8}}_{\text{degradation}} . \tag{2.27}$$

Similarly, we have that

$$\frac{dP_D^K}{dt} = \underbrace{\lambda_{P_D^K} K}_{\text{synthesis}} + \underbrace{\lambda_{Q_A} Q_A^K}_{\substack{\text{dissociation}\\ \text{of } Q_A^K}} + \underbrace{\lambda_Q Q^K}_{\substack{\text{dissociation}\\ \text{of } Q^K}} - \underbrace{\lambda_{P_D A_1} P_D^K A_1}_{\text{binding to } A_1} - \underbrace{\lambda_{P_D P_L} P_D^K P_L}_{\text{binding to } P_L} - \underbrace{d_{P_D} P_D^K}_{\text{degradation}} . \tag{2.28}$$

2.4.19 Equations for the PD-1/pembrolizumab Complex on Cells in the TS ($Q_A^{T_8}$ and Q_A^K)

Pembrolizumab binds to unbound PD-1 on the surfaces of PD-1-expressing cells in a 1:1 ratio [112], forming the PD-1/pembrolizumab complex in a reversible chemical process [113, 114]. We must also

account for loss due to the endocytosis and internalisation of the PD-1/pembrolizumab complex from the surface of cells [115, 116]. We assume that the rates of PD-1/pembrolizumab complex internalisation and dissociation are invariant of the type of cell expressing PD-1, so that

$$\frac{dQ_A^{T_8}}{dt} = \underbrace{\lambda_{P_D A_1} P_D^{T_8} A_1}_{\text{formation of } Q_A^{T_8}} - \underbrace{\lambda_{Q_A} Q_A^{T_8}}_{\text{dissociation of } Q_A^{T_8}} - \underbrace{d_{Q_A} Q_A^{T_8}}_{\text{internalisation}} , \tag{2.29}$$

$$\frac{dQ_A^{K}}{dt} = \underbrace{\lambda_{P_D A_1} P_D^{K} A_1}_{\text{formation of } Q_A^{K}} - \underbrace{\lambda_{Q_A} Q_A^{K}}_{\text{dissociation of } Q_A^{K}} - \underbrace{d_{Q_A} Q_A^{K}}_{\text{internalisation}} . \tag{2.30}$$

2.4.20 Equation for Pembrolizumab in the TS (A_1)

We assume that pembrolizumab is administered intravenously at times t_1, t_2, ..., t_n with doses ξ_1, ξ_2, ..., ξ_n respectively, assuming that the duration of infusion is negligible in comparison to the time period of interest. We also account for pembrolizumab depletion due to binding to unbound PD-1, replenishment due to PD-1/pembrolizumab complex dissociation, and elimination of pembrolizumab. It is important to note that the administered dose is not equal to the corresponding change in concentration in the TS. For simplicity, we assume linear pharmacokinetics so that, for some scaling factor f_{pembro}, we have that

$$\frac{dA_1}{dt} = \underbrace{\sum_{j=1}^{n} \xi_j f_{\text{pembro}} \delta\left(t - t_j\right)}_{\text{infusion}} + \underbrace{\lambda_{Q_A}\left(Q_A^{T_8} + Q_A^{K}\right)}_{\text{dissociation of } Q_A^{T_8} \text{ and } Q_A^{K}} - \underbrace{\lambda_{P_D A_1}\left(P_D^{T_8} + P_D^{K}\right) A_1}_{\text{formation of } Q_A^{T_8} \text{ and } Q_A^{K}} - \underbrace{d_{A_1} A_1}_{\text{elimination}} . \tag{2.31}$$

2.4.21 Equation for Unbound PD-L1 in the TS (P_L)

We also know that PD-L1 is expressed on the surface of viable cancer cells and M2 macrophages in the TS [117, 118]. We must take into account the synthesis of PD-L1, its depletion due to binding to unbound PD-1, replenishment due to PD-1/PD-L1 complex dissociation, and the degradation of PD-L1. Hence,

$$\frac{dP_L}{dt} = \underbrace{\lambda_{P_L C} C}_{\text{synthesis}} + \underbrace{\lambda_{P_L M_2} M_2}_{\text{synthesis}} + \underbrace{\lambda_{Q}\left(Q^{T_8} + Q^{K}\right)}_{\text{dissociation of } Q^{T_8} \text{ and } Q^{K}} - \underbrace{\lambda_{P_D P_L}\left(P_D^{T_8} + P_D^{K}\right) P_L}_{\text{formation of } Q^{T_8} \text{ and } Q^{K}} - \underbrace{d_{P_L} P_L}_{\text{degradation}} . \tag{2.32}$$

2.4.22 Equations for the PD-1/PD-L1 Complex in the TS (Q^{T_8} and Q^K)

PD-L1 binds to unbound PD-1 receptors on the surfaces of PD-1-expressing cells in a 1:1 ratio [119], forming the PD-1/PD-L1 complex in a reversible chemical process. Considering Q^{T_8} as an example, we can express its formation and dissociation via the reaction $P_D^{T_8} + P_L \underset{\lambda_Q}{\overset{\lambda_{P_D P_L}}{\rightleftharpoons}} Q^{T_8}$. We assume that the degradation is negligible relative to the dissociation, so that

$$\frac{dQ^{T_8}}{dt} = \underbrace{\lambda_{P_D P_L} P_D^{T_8} P_L}_{\text{formation}} - \underbrace{\lambda_{Q} Q^{T_8}}_{\text{dissociation}} . \tag{2.33}$$

However, the dissociation rate constant of the PD-1/PD-L1 complex is 1.44 s^{-1}, corresponding to a mean lifetime of less than 1 second [119]. As such, we employ a quasi-steady-state approximation

(QSSA) for Q^{T_8}, so that $\frac{dQ^{T_8}}{dt} = 0$, so that

$$Q^{T_8} = \frac{\lambda_{P_D P_L}}{\lambda_Q} P_D^{T_8} P_L. \tag{2.34}$$

Similarly,

$$Q^{K} = \frac{\lambda_{P_D P_L}}{\lambda_Q} P_D^{K} P_L. \tag{2.35}$$

Furthermore, we can simplify (2.27), (2.28), and (2.32) by substituting in (2.34) and (2.35), so that

$$\frac{dP_D^{T_8}}{dt} = \underbrace{\lambda_{P_D^{T_8}} T_8}_{\text{synthesis}} + \underbrace{\lambda_{Q_A} Q_A^{T_8}}_{\substack{\text{dissociation}\\ \text{of } Q_A^{T_8}}} - \underbrace{\lambda_{P_D A_1} P_D^{T_8} A_1}_{\text{binding to } A_1} - \underbrace{d_{P_D} P_D^{T_8}}_{\text{degradation}}, \tag{2.36}$$

$$\frac{dP_D^{K}}{dt} = \underbrace{\lambda_{P_D^{K}} K}_{\text{synthesis}} + \underbrace{\lambda_{Q_A} Q_A^{K}}_{\substack{\text{dissociation}\\ \text{of } Q_A^{K}}} - \underbrace{\lambda_{P_D A_1} P_D^{K} A_1}_{\text{binding to } A_1} - \underbrace{d_{P_D} P_D^{K}}_{\text{degradation}}, \tag{2.37}$$

$$\frac{dP_L}{dt} = \underbrace{\lambda_{P_L C} C}_{\text{synthesis}} + \underbrace{\lambda_{P_L M_2} M_2}_{\text{synthesis}} - \underbrace{d_{P_L} P_L}_{\text{degradation}}. \tag{2.38}$$

2.4.23 Equation for Unbound PD-1 receptors on Cells in the TDLN ($P_D^{8\text{LN}}$)

The equation for $P_D^{8\text{LN}}$ follows identically to that of (2.36). For simplicity, we assume that the formation and dissociation rates of the PD-1/pembrolizumab complex are identical in the TDLN and the TS so that

$$\frac{dP_D^{8\text{LN}}}{dt} = \underbrace{\lambda_{P_D^{8\text{LN}}} T_A^8}_{\text{synthesis}} + \underbrace{\lambda_{Q_A} Q_A^{8\text{LN}}}_{\substack{\text{dissociation}\\ \text{of } Q_A^{8\text{LN}}}} - \underbrace{\lambda_{P_D A_1} P_D^{8\text{LN}} A_1^{\text{LN}}}_{\text{binding to } A_1^{\text{LN}}} - \underbrace{d_{P_D} P_D^{8\text{LN}}}_{\text{degradation}}. \tag{2.39}$$

2.4.24 Equation for the PD-1/pembrolizumab Complex on Cells in the TDLN ($Q_A^{8\text{LN}}$)

The equation for $Q_A^{8\text{LN}}$ follows identically to that of (2.29). For simplicity, we assume that the rates of PD-1 receptor internalisation are identical in the TDLN and the TS, so that

$$\frac{dQ_A^{8\text{LN}}}{dt} = \underbrace{\lambda_{P_D A_1} P_D^{8\text{LN}} A_1^{\text{LN}}}_{\text{formation of } Q_A^{8\text{LN}}} - \underbrace{\lambda_{Q_A} Q_A^{8\text{LN}}}_{\text{dissociation of } Q_A^{8\text{LN}}} - \underbrace{d_{Q_A} Q_A^{8\text{LN}}}_{\text{internalisation}}. \tag{2.40}$$

2.4.25 Equation for Pembrolizumab in the TDLN (A_1^{LN})

The equation for A_1^{LN} follows identically to that of (2.31) so that

$$\frac{dA_1^{\text{LN}}}{dt} = \underbrace{\sum_{j=1}^{n} \xi_j f_{\text{pembro}} \delta(t - t_j)}_{\text{infusion}} + \underbrace{\lambda_{Q_A} Q_A^{8\text{LN}}}_{\text{dissociation of } Q_A^{8\text{LN}}} - \underbrace{\lambda_{P_D A_1} P_D^{8\text{LN}} A_1^{\text{LN}}}_{\text{formation of } Q_A^{8\text{LN}}} - \underbrace{d_{A_1} A_1^{\text{LN}}}_{\text{elimination}}. \tag{2.41}$$

2.4.26 Equation for Unbound PD-L1 in the TDLN (P_L^{LN})

We know that PD-L1 is expressed on the surface of mature DCs in the TDLN [120]. The equation for P_L^{LN} follows identically to (2.38) so that

$$\frac{dP_L^{\mathrm{LN}}}{dt} = \underbrace{\lambda_{P_L^{\mathrm{LN}} D^{\mathrm{LN}}} D^{\mathrm{LN}}}_{\text{synthesis}} - \underbrace{d_{P_L} P_L^{\mathrm{LN}}}_{\text{degradation}} . \tag{2.42}$$

2.4.27 Equations for the PD-1/PD-L1 Complex in the TDLN ($Q^{8\mathrm{LN}}$)

For simplicity, we assume that the formation and dissociation rates of the PD-1/PD-L1 complex are identical in the TDLN and the TS. The equation for $Q^{8\mathrm{LN}}$ follows identically from (2.34) so that

$$Q^{8\mathrm{LN}} = \frac{\lambda_{P_D P_L}}{\lambda_Q} P_D^{8\mathrm{LN}} P_L^{\mathrm{LN}}. \tag{2.43}$$

We note that throughout the model, the PD-1/PD-L1 complex appears only within an inhibition constant, making its absolute magnitude less important since it always appears as a ratio. One thing to note is that activated CD8+ T cells also express PD-1 receptors and PD-L1 ligands, and we assume that effector and activated cells express these in equal amounts. However, as discussed in [35], the ratio between effector and activated T cells can be assumed to remain roughly constant. Since the PD-1/PD-L1 complex concentration is linearly proportional to the product of PD-L1 concentration and unbound PD-1 receptor concentration, and PD-1/PD-L1-mediated inhibition of T cell proliferation in the TDLN appears only as a ratio, it is sufficient to consider only PD-1, PD-L1, and PD-1/PD-L1 concentrations on effector cells, as this will be appropriately scaled by the corresponding inhibition constants. Furthermore, this also justifies using the PD-1/PD-L1 complex concentration on effector T cells as a proxy for its concentration on activated T cells that have not yet undergone division, given that their ratio to effector cells remains roughly constant and that PD-1/PD-L1-mediated inhibition of T cell activation in the TDLN appears only as a ratio.

We also note that it is clear, from the structure of the model, that the non-negative orthant is positively forward invariant for all non-negative parameter choices, as the corresponding vector field is essentially non-negative; i.e., for each species X_i, if $X_i = 0$ with all other species non-negative, then $\frac{dX_i}{d_t} \geq 0$ because every negative term in $\frac{dX_i}{dt}$ contains X_i.

2.5 Model Reduction via QSSA

The model parameter values are estimated in Appendix B and are listed in Table B.5.

We observe that the degradation rates of cytokines are, in general, orders of magnitude larger than those of immune and cancer cells. In particular, IL-2, TNF, TGF-β, and IL-12 evolve on a very fast timescale, with degradation rates significantly higher than all other species in the model, causing them to equilibrate much more rapidly. Additionally, the combined death and migration rates of effector CD8+ T cells and Tregs, and the combined polarisation and death rates of naive macrophages, are much higher than the death rates of other model components, and compared with other model components, the PD-1/pembrolizumab complex undergoes dissociation or internalisation more rapidly. As such, we perform a QSSA and reduce the model by setting (2.9), (2.15), (2.17), (2.21) – (2.26), (2.29), (2.30), and (2.40) to 0 and solving for T_A^8, T_A^r, M_0, I_2, I_γ, I_α, I_β, I_{10}, I_{12}, $Q_A^{T_8}$, Q_A^K, and $Q_A^{8\mathrm{LN}}$ in terms of the other parameters and variables in the model. This minimally affects the system's evolution after

a very short period of transient behaviour [121], and we justify this by observing that, empirically, the deviation in system trajectories remains negligible for nearby parameter choices. Performing the QSSA leads to

$$\frac{dT_A^8}{dt} = 0 \implies T_A^8 = \frac{2^{n^8_{\max}} \exp\left(-d_{T_0^8}\tau_{T_A^8}\right) \lambda_{T_0^8 T_A^8} D^{\mathrm{LN}} T_0^8}{\left(\lambda_{T_A^8 T_8} + d_{T_8}\right)\left(1 + T_A^r/K_{T_0^8 T_A^r}\right)\left(1 + Q^{8\mathrm{LN}}/K_{T_0^8 Q^{8\mathrm{LN}}}\right)\left(1 + T_A^r/K_{T_A^8 T_A^r}\right)\left(1 + Q^{8\mathrm{LN}}/K_{T_A^8 Q^{8\mathrm{LN}}}\right)}, \tag{2.44}$$

$$\frac{dT_A^r}{dt} = 0 \implies T_A^r = \frac{2^{n^r_{\max}} \exp\left(-d_{T_0^r}\tau_{T_A^r}\right) \lambda_{T_0^r T_A^r}}{\lambda_{T_A^r T_r} + d_{T_r}} D^{\mathrm{LN}} T_0^r, \tag{2.45}$$

$$\frac{dM_0}{dt} = 0 \implies M_0 = \frac{\mathcal{A}_{M_0}}{\lambda_{M_1 I_\gamma}\frac{I_\gamma}{K_{M_1 I_\gamma}+I_\gamma} + \lambda_{M_1 I_\alpha}\frac{I_\alpha}{K_{M_1 I_\alpha}+I_\alpha} + \lambda_{M_2 I_\beta}\frac{I_\beta}{K_{M_2 I_\beta}+I_\beta} + \lambda_{M_2 I_{10}}\frac{I_{10}}{K_{M_2 I_{10}}+I_{10}} + d_{M_0}}, \tag{2.46}$$

$$\frac{dI_2}{dt} = 0 \implies I_2 = \frac{\lambda_{I_2 T_8}}{d_{I_2}} T_8, \tag{2.47}$$

$$\frac{dI_\gamma}{dt} = 0 \implies I_\gamma = \frac{\lambda_{I_\gamma K}}{d_{I_\gamma}} K, \tag{2.48}$$

$$\frac{dI_\alpha}{dt} = 0 \implies I_\alpha = \frac{1}{d_{I_\alpha}}\left(\lambda_{I_\alpha T_8} T_8 + \lambda_{I_\alpha K} K\right), \tag{2.49}$$

$$\frac{dI_\beta}{dt} = 0 \implies I_\beta = \frac{1}{d_{I_\beta}}\left(\lambda_{I_\beta C} C + \lambda_{I_\beta T_r} T_r\right), \tag{2.50}$$

$$\frac{dI_{10}}{dt} = 0 \implies I_{10} = \frac{\lambda_{I_{10} C}}{d_{I_{10}}} C, \tag{2.51}$$

$$\frac{dI_{12}}{dt} = 0 \implies I_{12} = \frac{\lambda_{I_{12} D}}{d_{I_{12}}} D, \tag{2.52}$$

$$\frac{dQ_A^{T_8}}{dt} = 0 \implies Q_A^{T_8} = \frac{\lambda_{P_D A_1}}{\lambda_{Q_A} + d_{Q_A}} P_D^{T_8} A_1, \tag{2.53}$$

$$\frac{dQ_A^{K}}{dt} = 0 \implies Q_A^{K} = \frac{\lambda_{P_D A_1}}{\lambda_{Q_A} + d_{Q_A}} P_D^{K} A_1, \tag{2.54}$$

$$\frac{dQ_A^{8\mathrm{LN}}}{dt} = 0 \implies Q_A^{8\mathrm{LN}} = \frac{\lambda_{P_D A_1}}{\lambda_{Q_A} + d_{Q_A}} P_D^{8\mathrm{LN}} A_1^{\mathrm{LN}}. \tag{2.55}$$

In particular, substituting (2.44), (2.45), and (2.53) – (2.55) into (2.10), (2.16), (2.36), (2.37), (2.60) (2.39), and (2.62), and simplifying, leads to

$$\begin{aligned}\frac{dT_8}{dt} = {} & \underbrace{\frac{V_{\mathrm{LN}}}{V_{\mathrm{TS}}}\lambda_{T_A^8 T_8} \frac{\exp\left(-d_{T_8}\tau_a\right) 2^{n^8_{\max}} \exp\left(-d_{T_0^8}\tau_{T_A^8}\right) \lambda_{T_0^8 T_A^8} D^{\mathrm{LN}} T_0^8}{\left(\lambda_{T_A^8 T_8} + d_{T_8}\right)\left(1 + T_A^r/K_{T_0^8 T_A^r}\right)\left(1 + Q^{8\mathrm{LN}}/K_{T_0^8 Q^{8\mathrm{LN}}}\right)\left(1 + T_A^r/K_{T_A^8 T_A^r}\right)\left(1 + Q^{8\mathrm{LN}}/K_{T_A^8 Q^{8\mathrm{LN}}}\right)}}_{T_A^8 \text{ migration to the TS}} \\ & + \underbrace{\lambda_{T_8 I_2}\frac{T_8 I_2}{K_{T_8 I_2} + I_2}\frac{1}{1 + T_r/K_{T_8 T_r}}}_{\text{growth by } I_2 \text{ inhibited by } T_r} - \underbrace{\lambda_{T_8 C}\frac{T_8 C}{K_{T_8 C} + C}}_{T_8 \to T_{\mathrm{ex}} \text{ from } C \text{ exposure}} + \underbrace{\lambda_{T_{\mathrm{ex}} A_1}\frac{T_{\mathrm{ex}} A_1}{K_{T_{\mathrm{ex}} A_1} + A_1}}_{T_{\mathrm{ex}} \to T_8 \text{ by } A_1} - \underbrace{\frac{d_{T_8} T_8}{1 + I_{10}/K_{T_8 I_{10}}}}_{\substack{\text{death} \\ \text{inhibited by } I_{10}}},\end{aligned} \tag{2.56}$$

$$\frac{dT_r}{dt} = \underbrace{\frac{V_{\text{LN}}}{V_{\text{TS}}}\lambda_{T_A^r T_r}\exp\left(-d_{T_r}\tau_a\right)\frac{2^{n^r_{\max}}\exp\left(-d_{T_0^r}\tau_{T_A^r}\right)\lambda_{T_0^r T_A^r}}{\lambda_{T_A^r T_r}+d_{T_r}}D^{\text{LN}}T_0^r}_{T_A^r \text{ migration to the TS}} - \underbrace{d_{T_r}T_r}_{\text{death}}, \tag{2.57}$$

$$\frac{dP_D^{T_8}}{dt} = \underbrace{\lambda_{P_D^{T_8}}T_8}_{\text{synthesis}} - \underbrace{\lambda_{P_D A_1}\frac{d_{Q_A}}{\lambda_{Q_A}+d_{Q_A}}P_D^{T_8}A_1}_{\text{formation and dissociation of } Q_A^{T_8}} - \underbrace{d_{P_D}P_D^{T_8}}_{\text{degradation}}, \tag{2.58}$$

$$\frac{dP_D^{K}}{dt} = \underbrace{\lambda_{P_D^{K}}K}_{\text{synthesis}} - \underbrace{\lambda_{P_D A_1}\frac{d_{Q_A}}{\lambda_{Q_A}+d_{Q_A}}P_D^{K}A_1}_{\text{formation and dissociation of } Q_A^{K}} - \underbrace{d_{P_D}P_D^{K}}_{\text{degradation}}, \tag{2.59}$$

$$\frac{dA_1}{dt} = \underbrace{\sum_{j=1}^{n}\xi_j f_{\text{pembro}}\delta\left(t-t_j\right)}_{\text{infusion}} - \underbrace{\lambda_{P_D A_1}\frac{d_{Q_A}}{\lambda_{Q_A}+d_{Q_A}}\left(P_D^{T_8}+P_D^{K}\right)A_1}_{\text{formation and dissociation of } Q_A^{T_8} \text{ and } Q_A^{K}} - \underbrace{d_{A_1}A_1}_{\text{elimination}}, \tag{2.60}$$

$$\frac{dP_D^{8\text{LN}}}{dt} = \underbrace{\lambda_{P_D^{8\text{LN}}}T_A^8}_{\text{synthesis}} - \underbrace{\lambda_{P_D A_1}\frac{d_{Q_A}}{\lambda_{Q_A}+d_{Q_A}}P_D^{8\text{LN}}A_1^{\text{LN}}}_{\text{formation and dissociation of } Q_A^{8\text{LN}}} - \underbrace{d_{P_D}P_D^{8\text{LN}}}_{\text{degradation}}, \tag{2.61}$$

$$\frac{dA_1^{\text{LN}}}{dt} = \underbrace{\sum_{j=1}^{n}\xi_j f_{\text{pembro}}\delta\left(t-t_j\right)}_{\text{infusion}} + \underbrace{\lambda_{P_D A_1}\frac{d_{Q_A}}{\lambda_{Q_A}+d_{Q_A}}P_D^{8\text{LN}}A_1^{\text{LN}}}_{\text{formation and dissociation of } Q_A^{8\text{LN}}} - \underbrace{d_{A_1}A_1^{\text{LN}}}_{\text{elimination}}. \tag{2.62}$$

2.6 Conversion to an Agent-Based Model

To convert the ODE-based model to an ABM, we must realise that one-to-one agent representation of all biological entities is computationally intractable. As such, we first nondimensionalise the governing equations and model components, choosing parameter rescalings such that the original model's structure is preserved. For each model species, X, we introduce a scaling factor, g_X, and define the non-dimensional equivalent species, $\tilde{X}$, via $X := g_X\tilde{X}$. Then, substituting this into the model and simplifying leads to

$$\begin{aligned}\frac{d\tilde{C}}{dt} &= \lambda_C\tilde{C}\left(1-\frac{\tilde{C}}{\tilde{C}_0}\right) - \tilde{\lambda}_{CT_8}\tilde{T}_8\frac{1}{1+\tilde{I}_\beta/\tilde{K}_{CI_\beta}}\frac{1}{1+\tilde{Q}^{T_8}/\tilde{K}_{CQ^{T_8}}}\tilde{C}\\ &\quad - \tilde{\lambda}_{CK}\tilde{K}\frac{1}{1+\tilde{I}_\beta/\tilde{K}_{CI_\beta}}\frac{1}{1+\tilde{Q}^{K}/\tilde{K}_{CQ^{K}}}\tilde{C} - \lambda_{CI_\alpha}\frac{\tilde{I}_\alpha}{\tilde{K}_{CI_\alpha}+\tilde{I}_\alpha}\tilde{C},\end{aligned} \tag{2.63}$$

$$\frac{d\tilde{N}_c}{dt} = \tilde{\lambda}_{CI_\alpha}\frac{\tilde{I}_\alpha}{\tilde{K}_{CI_\alpha}+\tilde{I}_\alpha}\tilde{C} - d_{N_c}\tilde{N}_c, \tag{2.64}$$

$$\frac{d\tilde{D}_0}{dt} = \tilde{\mathcal{A}}_{D_0} - \lambda_{DN_c}\tilde{D}_0\frac{\tilde{N}_c}{\tilde{K}_{DN_c}+\tilde{N}_c} - \tilde{\lambda}_{D_0K}\tilde{D}_0\tilde{K}\frac{1}{1+\tilde{I}_\beta/\tilde{K}_{D_0I_\beta}} - d_{D_0}\tilde{D}_0, \tag{2.65}$$

$$\frac{d\tilde{D}}{dt} = \tilde{\lambda}_{DN_c}\tilde{D}_0\frac{\tilde{N}_c}{\tilde{K}_{DN_c}+\tilde{N}_c} - \lambda_{DD^{\text{LN}}}\tilde{D} - d_D\tilde{D}, \tag{2.66}$$

$$\frac{d\tilde{D}^{\text{LN}}}{dt} = \frac{V_{\text{TS}}}{V_{\text{LN}}}\tilde{\lambda}_{DD^{\text{LN}}}\exp\left(-d_D\tau_m\right)\tilde{D} - d_D\tilde{D}^{\text{LN}}, \tag{2.67}$$

$$\frac{d\tilde{T}_0^8}{dt} = \mathcal{A}_{T_0^8}/g_{T_0^8} - \tilde{\lambda}_{T_0^8 T_A^8}\tilde{R}^8 - d_{T_0^8}\tilde{T}_0^8, \tag{2.68}$$

where $\tilde{R}^8$ is defined as

$$\tilde{R}^8 := \frac{\tilde{D}^{\mathrm{LN}}\tilde{T}_0^8}{\left(1+\tilde{T}_A^r/\tilde{K}_{T_0^8 T_A^r}\right)\left(1+\tilde{Q}^{8\mathrm{LN}}/\tilde{K}_{T_0^8 Q^{8\mathrm{LN}}}\right)}, \tag{2.69}$$

$$\tilde{T}_A^8 = \frac{2^{n_{\max}^8}\exp\left(-d_{T_0^8}\tau_{T_A^8}\right)\hat{\lambda}_{T_0^8 T_A^8}\tilde{R}^8}{\left(\lambda_{T_A^8 T_8}+d_{T_8}\right)\left(1+\tilde{T}_A^r/\tilde{K}_{T_A^8 T_A^r}\right)\left(1+\tilde{Q}^{8\mathrm{LN}}/\tilde{K}_{T_A^8 Q^{8\mathrm{LN}}}\right)}, \tag{2.70}$$

$$\begin{aligned}\frac{d\tilde{T}_8}{dt} &= \frac{V_{\mathrm{LN}}}{V_{\mathrm{TS}}}\tilde{\lambda}_{T_A^8 T_8}\exp\left(-d_{T_8}\tau_a\right)\frac{2^{n_{\max}^8}\exp\left(-d_{T_0^8}\tau_{T_A^8}\right)\hat{\lambda}_{T_0^8 T_A^8}\tilde{R}^8}{\left(\lambda_{T_A^8 T_8}+d_{T_8}\right)\left(1+\tilde{T}_A^r/\tilde{K}_{T_A^8 T_A^r}\right)\left(1+\tilde{Q}^{8\mathrm{LN}}/\tilde{K}_{T_A^8 Q^{8\mathrm{LN}}}\right)} \\ &\quad + \lambda_{T_8 I_2}\frac{\tilde{T}_8\tilde{I}_2}{\tilde{K}_{T_8 I_2}+\tilde{I}_2}\frac{1}{1+\tilde{T}_r/\tilde{K}_{T_8 T_r}} - \lambda_{T_8 C}\frac{\tilde{T}_8\tilde{C}}{\tilde{K}_{T_8 C}+\tilde{C}} + \tilde{\lambda}_{T_{\mathrm{ex}} A_1}\frac{\tilde{T}_{\mathrm{ex}}\tilde{A}_1}{\tilde{K}_{T_{\mathrm{ex}} A_1}+\tilde{A}_1} - \frac{d_{T_8}\tilde{T}_8}{1+\tilde{I}_{10}/\tilde{K}_{T_8 I_{10}}},\end{aligned} \tag{2.71}$$

$$\frac{d\tilde{T}_{\mathrm{ex}}}{dt} = \tilde{\lambda}_{T_8 C}\frac{\tilde{T}_8\tilde{C}}{\tilde{K}_{T_8 C}+\tilde{C}} - \lambda_{T_{\mathrm{ex}} A_1}\frac{\tilde{T}_{\mathrm{ex}}\tilde{A}_1}{\tilde{K}_{T_{\mathrm{ex}} A_1}+\tilde{A}_1} - \frac{d_{T_{\mathrm{ex}}}\tilde{T}_{\mathrm{ex}}}{1+\tilde{I}_{10}/\tilde{K}_{T_{\mathrm{ex}} I_{10}}}, \tag{2.72}$$

$$\frac{d\tilde{T}_0^r}{dt} = \tilde{\mathcal{A}}_{T_0^r} - \tilde{\lambda}_{T_0^r T_A^r}\tilde{R}^r - d_{T_0^r}\tilde{T}_0^r, \tag{2.73}$$

where $\tilde{R}^r$ is defined as

$$\tilde{R}^r := \tilde{D}^{\mathrm{LN}}\tilde{T}_0^r, \tag{2.74}$$

$$\tilde{T}_A^r = \frac{2^{n_{\max}^r}\exp\left(-d_{T_0^r}\tau_{T_A^r}\right)\hat{\lambda}_{T_0^r T_A^r}\tilde{R}^r}{\lambda_{T_A^r T_r}+d_{T_r}}, \tag{2.75}$$

$$\frac{d\tilde{T}_r}{dt} = \frac{V_{\mathrm{LN}}}{V_{\mathrm{TS}}}\tilde{\lambda}_{T_A^r T_r}\exp\left(-d_{T_r}\tau_a\right)\frac{2^{n_{\max}^r}\exp\left(-d_{T_0^r}\tau_{T_A^r}\right)\hat{\lambda}_{T_0^r T_A^r}\tilde{R}^r}{\lambda_{T_A^r T_r}+d_{T_r}} - d_{T_r}\tilde{T}_r, \tag{2.76}$$

$$\tilde{M}_0 = \frac{\tilde{\mathcal{A}}_{M_0}}{\lambda_{M_1 I_\gamma}\frac{\tilde{I}_\gamma}{\tilde{K}_{M_1 I_\gamma}+\tilde{I}_\gamma} + \lambda_{M_1 I_\alpha}\frac{\tilde{I}_\alpha}{\tilde{K}_{M_1 I_\alpha}+\tilde{I}_\alpha} + \lambda_{M_2 I_\beta}\frac{\tilde{I}_\beta}{\tilde{K}_{M_2 I_\beta}+\tilde{I}_\beta} + \lambda_{M_2 I_{10}}\frac{\tilde{I}_{10}}{\tilde{K}_{M_2 I_{10}}+\tilde{I}_{10}} + d_{M_0}}, \tag{2.77}$$

$$\frac{d\tilde{M}_2}{dt} = \tilde{\lambda}_{M_2 I_\beta}\tilde{M}_0\frac{\tilde{I}_\beta}{\tilde{K}_{M_2 I_\beta}+\tilde{I}_\beta} + \tilde{\lambda}_{M_2 I_{10}}\tilde{M}_0\frac{\tilde{I}_{10}}{\tilde{K}_{M_2 I_{10}}+\tilde{I}_{10}} - d_{M_2}\tilde{M}_2, \tag{2.78}$$

$$\frac{d\tilde{K}_0}{dt} = \tilde{\mathcal{A}}_{K_0} - \left(\lambda_{K I_2}\tilde{K}_0\frac{\tilde{I}_2}{\tilde{K}_{K I_2}+\tilde{I}_2} + \lambda_{K I_{12}}\tilde{K}_0\frac{\tilde{I}_{12}}{\tilde{K}_{K I_{12}}+\tilde{I}_{12}}\right)\frac{1}{1+\tilde{I}_\beta/\tilde{K}_{K I_\beta}} - d_{K_0}\tilde{K}_0, \tag{2.79}$$

$$\frac{d\tilde{K}}{dt} = \left(\tilde{\lambda}_{K I_2}\tilde{K}_0\frac{\tilde{I}_2}{\tilde{K}_{K I_2}+\tilde{I}_2} + \tilde{\lambda}_{K I_{12}}\tilde{K}_0\frac{\tilde{I}_{12}}{\tilde{K}_{K I_{12}}+\tilde{I}_{12}}\right)\frac{1}{1+\tilde{I}_\beta/\tilde{K}_{K I_\beta}} - d_K\tilde{K}, \tag{2.80}$$

$$\tilde{I}_2 = \frac{\tilde{\lambda}_{I_2 T_8}}{d_{I_2}}\tilde{T}_8, \tag{2.81}$$

$$\tilde{I}_\gamma = \frac{\tilde{\lambda}_{I_\gamma K}}{d_{I_\gamma}}\tilde{K}, \tag{2.82}$$

$$\tilde{I}_\alpha = \frac{1}{d_{I_\alpha}}\left[\tilde{\lambda}_{I_\alpha T_8}\tilde{T}_8 + \tilde{\lambda}_{I_\alpha K}\tilde{K}\right], \tag{2.83}$$

$$\tilde{I}_\beta = \frac{1}{d_{I_\beta}}\left[\tilde{\lambda}_{I_\beta C}\tilde{C} + \tilde{\lambda}_{I_\beta M_2}\tilde{M}_2\right], \tag{2.84}$$

$$\tilde{I}_{10} = \frac{\tilde{\lambda}_{I_{10}C}}{d_{I_{10}}}\tilde{C}, \tag{2.85}$$

$$\tilde{I}_{12} = \frac{\tilde{\lambda}_{I_{12}D}}{d_{I_{12}}}\tilde{D}, \tag{2.86}$$

$$\frac{d\tilde{P}_D^{T_8}}{dt} = \tilde{\lambda}_{P_D^{T_8}}\tilde{T}_8 - \lambda_{P_D^{T_8}A_1}\tilde{P}_D^{T_8}\tilde{A}_1 - d_{P_D}\tilde{P}_D^{T_8}, \tag{2.87}$$

$$\frac{d\tilde{P}_D^{K}}{dt} = \tilde{\lambda}_{P_D^{K}}\tilde{K} - \lambda_{P_D^{K}A_1}\tilde{P}_D^{K}\tilde{A}_1 - d_{P_D}\tilde{P}_D^{K}, \tag{2.88}$$

$$\tilde{Q}_A^{T_8} = \frac{\hat{\lambda}_{P_D^{T_8}A_1}}{\lambda_{Q_A} + d_{Q_A}}\tilde{P}_D^{T_8}\tilde{A}_1, \tag{2.89}$$

$$\tilde{Q}_A^{K} = \frac{\hat{\lambda}_{P_D^{K}A_1}}{\lambda_{Q_A} + d_{Q_A}}\tilde{P}_D^{K}\tilde{A}_1, \tag{2.90}$$

$$\frac{d\tilde{A}_1}{dt} = \sum_{j=1}^{n}\xi_j f_{\mathrm{pembro}A_1}\delta(t-t_j) - \left(\tilde{\lambda}_{P_D^{T_8}A_1}\tilde{P}_D^{T_8} + \tilde{\lambda}_{P_D^{K}A_1}\tilde{P}_D^{K}\right)\tilde{A}_1 - d_{A_1}\tilde{A}_1, \tag{2.91}$$

$$\frac{d\tilde{P}_L}{dt} = \tilde{\lambda}_{P_L C}\tilde{C} + \tilde{\lambda}_{P_L M_2}\tilde{M}_2 - d_{P_L}\tilde{P}_L, \tag{2.92}$$

$$\tilde{Q}^{T_8} = \frac{\lambda_{P_D^{T_8}P_L}}{\lambda_Q}\tilde{P}_D^{T_8}\tilde{P}_L, \tag{2.93}$$

$$\tilde{Q}^{K} = \frac{\lambda_{P_D^{K}P_L}}{\lambda_Q}\tilde{P}_D^{K}\tilde{P}_L, \tag{2.94}$$

$$\frac{d\tilde{P}_D^{8\mathrm{LN}}}{dt} = \tilde{\lambda}_{P_D^{8\mathrm{LN}}}\tilde{T}_A^8 - \lambda_{P_D^{8\mathrm{LN}}A_1^{\mathrm{LN}}}\tilde{P}_D^{8\mathrm{LN}}\tilde{A}_1^{\mathrm{LN}} - d_{P_D}\tilde{P}_D^{8\mathrm{LN}}, \tag{2.95}$$

$$\tilde{Q}_A^{8\mathrm{LN}} = \frac{\hat{\lambda}_{P_D^{8\mathrm{LN}}A_1^{\mathrm{LN}}}}{\lambda_{Q_A} + d_{Q_A}}\tilde{P}_D^{8\mathrm{LN}}\tilde{A}_1^{\mathrm{LN}}, \tag{2.96}$$

$$\frac{d\tilde{A}_1^{\mathrm{LN}}}{dt} = \sum_{j=1}^{n}\xi_j f_{\mathrm{pembro}A_1^{\mathrm{LN}}}\delta(t-t_j) - \tilde{\lambda}_{P_D^{8\mathrm{LN}}A_1^{\mathrm{LN}}}\tilde{P}_D^{8\mathrm{LN}}\tilde{A}_1^{\mathrm{LN}} - d_{A_1}\tilde{A}_1^{\mathrm{LN}}, \tag{2.97}$$

$$\frac{d\tilde{P}_L^{\mathrm{LN}}}{dt} = \tilde{\lambda}_{P_L^{\mathrm{LN}}D^{\mathrm{LN}}}\tilde{D}^{\mathrm{LN}} - d_{P_L}\tilde{P}_L^{\mathrm{LN}}, \tag{2.98}$$

$$\tilde{Q}^{8\mathrm{LN}} = \frac{\lambda_{P_D^{8\mathrm{LN}}P_L^{\mathrm{LN}}}}{\lambda_Q}\tilde{P}_D^{8\mathrm{LN}}\tilde{P}_L^{\mathrm{LN}}, \tag{2.99}$$

with scalings of

$$\tilde{C}_0 = C_0/g_C, \qquad \tilde{\lambda}_{CT_8} = \lambda_{CT_8}g_{T_8}, \qquad \tilde{K}_{CI_\beta} = K_{CI_\beta}/g_{I_\beta},$$

$$\tilde{K}_{CQ^{T_8}} = K_{CQ^{T_8}}/g_{Q^{T_8}}, \qquad \tilde{\lambda}_{CK} = \lambda_{CK}g_K, \qquad \tilde{K}_{CQ^K} = K_{CQ^K}/g_{Q^K},$$

$$\tilde{K}_{CI_\alpha} = K_{CI_\alpha}/g_{I_\alpha}, \qquad \tilde{\lambda}_{CI_\alpha} = \lambda_{CI_\alpha}\frac{g_C}{g_{N_c}}, \qquad \tilde{\mathcal{A}}_{D_0} = \mathcal{A}_{D_0}/g_{D_0},$$

$$\tilde{K}_{DN_c} = K_{DN_c}/g_{N_c}, \qquad \tilde{\lambda}_{D_0K} = \lambda_{D_0K}g_K, \qquad \tilde{K}_{D_0I_\beta} = K_{D_0I_\beta}/g_{I_\beta},$$

$$\tilde{\lambda}_{DN_c} = \lambda_{DN_c}\frac{g_{D_0}}{g_D}, \qquad \tilde{\lambda}_{DD^{\mathrm{LN}}} = \lambda_{DD^{\mathrm{LN}}}\frac{g_D}{g_{D^{\mathrm{LN}}}}, \qquad \tilde{\mathcal{A}}_{T_0^8} = \mathcal{A}_{T_0^8}/g_{T_0^8},$$

$$\tilde{\lambda}_{T_0^8T_A^8} = \lambda_{T_0^8T_A^8}g_{D^{\mathrm{LN}}}, \qquad \tilde{K}_{T_0^8T_A^r} = K_{T_0^8T_A^r}/g_{T_A^r}, \qquad \tilde{K}_{T_0^8Q^{8\mathrm{LN}}} = K_{T_0^8Q^{8\mathrm{LN}}}/g_{Q^{8\mathrm{LN}}},$$

$$\hat{\lambda}_{T_0^8T_A^8} = \lambda_{T_0^8T_A^8}\frac{g_{D^{\mathrm{LN}}}g_{T_0^8}}{g_{T_A^8}}, \qquad \tilde{K}_{T_A^8T_A^r} = K_{T_A^8T_A^r}/g_{T_A^r}, \qquad \tilde{K}_{T_A^8Q^{8\mathrm{LN}}} = K_{T_A^8Q^{8\mathrm{LN}}}/g_{Q^{8\mathrm{LN}}},$$

$$\tilde{\lambda}_{T_A^8T_8} = \lambda_{T_A^8T_8}\frac{g_{T_A^8}}{g_{T_8}}, \qquad \tilde{K}_{T_8I_2} = K_{T_8I_2}/g_{I_2}, \qquad \tilde{K}_{T_8T_r} = K_{T_8T_r}/g_{T_r},$$

$$\tilde{K}_{T_8C} = K_{T_8C}/g_C, \qquad \tilde{\lambda}_{T_{\mathrm{ex}}A_1} = \lambda_{T_{\mathrm{ex}}A_1}\frac{g_{T_{\mathrm{ex}}}}{g_{T_8}}, \qquad \tilde{K}_{T_{\mathrm{ex}}A_1} = K_{T_{\mathrm{ex}}A_1}/g_{A_1},$$

$$\tilde{K}_{T_8I_{10}} = K_{T_8I_{10}}/g_{I_{10}}, \qquad \tilde{\lambda}_{T_8C} = \lambda_{T_8C}\frac{g_{T_8}}{g_{T_{\mathrm{ex}}}}, \qquad \tilde{K}_{T_{\mathrm{ex}}I_{10}} = K_{T_{\mathrm{ex}}I_{10}}/g_{I_{10}},$$

$$\tilde{\mathcal{A}}_{T_0^r} = \mathcal{A}_{T_0^r}/g_{T_0^r}, \qquad \tilde{\lambda}_{T_0^rT_A^r} = \lambda_{T_0^rT_A^r}g_{D^{\mathrm{LN}}}, \qquad \hat{\lambda}_{T_0^rT_A^r} = \lambda_{T_0^rT_A^r}\frac{g_{D^{\mathrm{LN}}}g_{T_0^r}}{g_{T_A^r}},$$

$$\tilde{\lambda}_{T_A^rT_r} = \lambda_{T_A^rT_r}\frac{g_{T_A^r}}{g_{T_r}}, \qquad \tilde{\mathcal{A}}_{M_0} = \mathcal{A}_{M_0}/g_{M_0}, \qquad \tilde{K}_{M_2I_\beta} = K_{M_2I_\beta}/g_{I_\beta},$$

$$\tilde{K}_{M_1I_\gamma} = K_{M_1I_\gamma}/g_{I_\gamma}, \qquad \tilde{K}_{M_1I_\alpha} = K_{M_1I_\alpha}/g_{I_\alpha}, \qquad \tilde{K}_{M_2I_{10}} = K_{M_2I_{10}}/g_{I_{10}},$$

$$\tilde{\lambda}_{M_2I_\beta} = \lambda_{M_2I_\beta}\frac{g_{M_0}}{g_{M_2}}, \qquad \tilde{\lambda}_{M_2I_{10}} = \lambda_{M_2I_{10}}\frac{g_{M_0}}{g_{M_2}}, \qquad \tilde{\mathcal{A}}_{K_0} = \mathcal{A}_{K_0}/g_{K_0},$$

$$\tilde{K}_{KI_2} = K_{KI_2}/g_{I_2}, \qquad \tilde{K}_{KI_{12}} = K_{KI_{12}}/g_{I_{12}}, \qquad \tilde{K}_{KI_\beta} = K_{KI_\beta}/g_{I_\beta},$$

$$\tilde{\lambda}_{KI_2} = \lambda_{KI_2}\frac{g_{K_0}}{g_K}, \qquad \tilde{\lambda}_{KI_{12}} = \lambda_{KI_{12}}\frac{g_{K_0}}{g_K}, \qquad \tilde{\lambda}_{I_2T_8} = \lambda_{I_2T_8}\frac{g_{T_8}}{g_{I_2}},$$

$$\tilde{\lambda}_{I_\gamma K} = \lambda_{I_\gamma K}\frac{g_K}{g_{I_\gamma}}, \qquad \tilde{\lambda}_{I_\alpha T_8} = \lambda_{I_\alpha T_8}\frac{g_{T_8}}{g_{I_\alpha}}, \qquad \tilde{\lambda}_{I_\alpha K} = \lambda_{I_\alpha K}\frac{g_K}{g_{I_\alpha}},$$

$$\tilde{\lambda}_{I_\beta C} = \lambda_{I_\beta C}\frac{g_C}{g_{I_\beta}}, \qquad \tilde{\lambda}_{I_\beta M_2} = \lambda_{I_\beta M_2}\frac{g_{M_2}}{g_{I_\beta}}, \qquad \tilde{\lambda}_{I_{10}C} = \lambda_{I_{10}C}\frac{g_C}{g_{I_{10}}},$$

$$\tilde{\lambda}_{I_{12}D} = \lambda_{I_{12}D}\frac{g_D}{g_{I_{12}}}, \qquad \tilde{\lambda}_{P_D^{T_8}} = \lambda_{P_D^{T_8}}\frac{g_{T_8}}{g_{P_D^{T_8}}}, \qquad \lambda_{P_D^{T_8}A_1} = \lambda_{P_DA_1}\frac{d_{Q_A}}{\lambda_{Q_A}+d_{Q_A}}g_{A_1},$$

$$\lambda_{P_D^KA_1} = \lambda_{P_DA_1}\frac{d_{Q_A}}{\lambda_{Q_A}+d_{Q_A}}g_{A_1}, \qquad \hat{\lambda}_{P_D^{T_8}A_1} = \lambda_{P_DA_1}\frac{g_{P_D^{T_8}}g_{A_1}}{g_{Q_A^{T_8}}}, \qquad \hat{\lambda}_{P_D^KA_1} = \lambda_{P_DA_1}\frac{g_{P_D^K}g_{A_1}}{g_{Q_A^K}},$$

$$f_{\mathrm{pembro}A_1} = \frac{f_{\mathrm{pembro}}}{g_{A_1}}, \qquad \tilde{\lambda}_{P_D^{T_8}A_1} = \lambda_{P_DA_1}\frac{d_{Q_A}}{\lambda_{Q_A}+d_{Q_A}}g_{P_D^{T_8}}, \qquad \tilde{\lambda}_{P_D^KA_1} = \lambda_{P_DA_1}\frac{d_{Q_A}}{\lambda_{Q_A}+d_{Q_A}}g_{P_D^K},$$

$$\tilde{\lambda}_{P_LC} = \lambda_{P_LC}\frac{g_C}{g_{P_L}}, \qquad \tilde{\lambda}_{P_LM_2} = \lambda_{P_LM_2}\frac{g_{M_2}}{g_{P_L}}, \qquad \lambda_{P_D^{T_8}P_L} = \lambda_{P_DP_L}\frac{g_{P_D^{T_8}}g_{P_L}}{g_{Q^{T_8}}},$$

$$\lambda_{P_D^KP_L} = \lambda_{P_DP_L}\frac{g_{P_D^K}g_{P_L}}{g_{Q^K}}, \qquad \tilde{\lambda}_{P_D^{8\mathrm{LN}}} = \lambda_{P_D^{8\mathrm{LN}}}\frac{g_{T_A^8}}{g_{P_D^{8\mathrm{LN}}}}, \qquad \lambda_{P_D^{8\mathrm{LN}}A_1^{\mathrm{LN}}} = \lambda_{P_DA_1}\frac{d_{Q_A}}{\lambda_{Q_A}+d_{Q_A}}g_{A_1^{\mathrm{LN}}},$$

$$\hat{\lambda}_{P_D^{8\mathrm{LN}}A_1^{\mathrm{LN}}} = \lambda_{P_DA_1}\frac{g_{P_D^{8\mathrm{LN}}}g_{A_1^{\mathrm{LN}}}}{g_{Q^{8\mathrm{LN}}}}, \qquad f_{\mathrm{pembro}A_1^{\mathrm{LN}}} = \frac{f_{\mathrm{pembro}}}{g_{A_1^{\mathrm{LN}}}}, \qquad \tilde{\lambda}_{P_D^{8\mathrm{LN}}A_1^{\mathrm{LN}}} = \lambda_{P_DA_1}\frac{d_{Q_A}}{\lambda_{Q_A}+d_{Q_A}}g_{P_D^{8\mathrm{LN}}},$$

$$\tilde{\lambda}_{P_L^{\mathrm{LN}}D^{\mathrm{LN}}} = \lambda_{P_L^{\mathrm{LN}}D^{\mathrm{LN}}}\frac{g_{D^{\mathrm{LN}}}}{g_{P_L^{\mathrm{LN}}}}, \qquad \tilde{\lambda}_{P_L^{\mathrm{LN}}T_A^r} = \lambda_{P_L^{\mathrm{LN}}T_A^r}\frac{g_{T_A^r}}{g_{P_L^{\mathrm{LN}}}}, \qquad \lambda_{P_D^{8\mathrm{LN}}P_L^{\mathrm{LN}}} = \lambda_{P_DP_L}\frac{g_{P_D^{8\mathrm{LN}}}g_{P_L^{\mathrm{LN}}}}{g_{Q^{8\mathrm{LN}}}}.$$

A derivation of this is shown in Appendix A, noting that we do not non-dimensionalise time, but refer to parameters as non-dimensionalised nonetheless.

For simplicity, we evolve the ABM on a uniform temporal grid, with spacing Δt, employing a time-driven, synchronous update scheme for agent states and concentrations, which we now detail. Specifi-

cally, at each time step, a continuous-time event with rate λ is mapped to a per-step occurrence probability $p = 1 - \exp(-\lambda \Delta t)$. We then perform a Bernoulli(p) trial, equivalently sampling $X \sim \mathcal{U}[0,1]$ and triggering the event if $X \leq p$, to decide whether the event occurs for a given agent, after which the corresponding state-transition rule is applied. This construction is consistent with considering $T \sim \text{Exp}(\lambda)$, an exponential distribution with rate constant λ, since $p = \Pr[T \leq \Delta t] = 1 - \exp(-\lambda \Delta t)$, with T being interpreted as the waiting time for the corresponding continuous process to occur. In the mean-field limit, this yields a scheme that is the ABM analogue of the first-order forward Euler method for integrating the governing ODEs.

Processes in the ODE model can be organised into three categories: a) source/supply processes that introduce agents; b) loss processes that remove agents, such as degradation and lysis, and c) state transitions that change agent states (e.g., migration, activation, maturation, exhaustion, necrosis, complex formation/dissociation). For clarity, we provide examples of processes from each category, and explain how these are converted from the corresponding ODEs to the ABM.

We first consider the constant supply of immature DCs, with non-dimensionalised supply rate $\tilde{\mathcal{A}}_{D_0}$. This is equivalent to supplying $\tilde{\mathcal{A}}_{D_0} \Delta t$ immature DCs at each time step. Taking into account the discrete nature of agents, this is equivalent to introducing $\left\lfloor \tilde{\mathcal{A}}_{D_0} \Delta t \right\rfloor + X$ agents corresponding to $\tilde{D}_0$, where $X \sim \text{Bernoulli}(\{\tilde{\mathcal{A}}_{D_0} \Delta t\})$. Here, $\lfloor \cdot \rfloor$ denotes the floor function, while $\{\cdot\}$ denotes the fractional part function, so that $x = \lfloor x \rfloor + \{x\}$ for all $x \in \mathbb{R}$. We next translate the synthesis of PD-1 on the surface of NK cells, represented with non-dimensionalised rate constant $\tilde{\lambda}_{P_D^K}$. As such, for each activated NK cell agent, at each time step, we sample $X \sim \text{Bernoulli}\left(1 - \exp\left(-\tilde{\lambda}_{P_D^K} \Delta t\right)\right)$. If $X = 1$, then we spawn an agent corresponding to $\tilde{P}_D^K$.

Considering loss processes, we focus on the degradation of exhausted CD8+ T cells, which occurs with a non-dimensionalised rate $\frac{d_{T_{\text{ex}}}}{1+\tilde{I}_{10}/\tilde{K}_{T_{\text{ex}} I_{10}}}$. As such, at each time point, for each exhausted CD8+ T cell agent, we sample $X \sim \text{Bernoulli}\left(1 - \exp\left(-\frac{d_{T_{\text{ex}}}}{1+\tilde{I}_{10}/\tilde{K}_{T_{\text{ex}} I_{10}}} \Delta t\right)\right)$, and if $X = 1$, then we remove the corresponding agent.

Finally, we consider processes involving transitions between agent states, which are amongst the most interesting and complex to implement. We consider the necrosis of viable cancer cells by TNF, which occurs with non-dimensionalised rate $\lambda_{CI_\alpha} \frac{\tilde{I}_\alpha}{\tilde{K}_{CI_\alpha} + \tilde{I}_\alpha}$. As such, at each time point, for each viable cancer cell agent, we sample $X \sim \text{Bernoulli}\left(1 - \exp\left(-\lambda_{CI_\alpha} \frac{\tilde{I}_\alpha}{\tilde{K}_{CI_\alpha} + \tilde{I}_\alpha} \Delta t\right)\right)$. If $X = 1$, then we kill the corresponding agent, and spawn $\tilde{\lambda}_{CI_\alpha} \frac{\tilde{I}_\alpha}{\tilde{K}_{CI_\alpha} + \tilde{I}_\alpha} \div \lambda_{CI_\alpha} \frac{\tilde{I}_\alpha}{\tilde{K}_{CI_\alpha} + \tilde{I}_\alpha} = \frac{\tilde{\lambda}_{CI_\alpha}}{\lambda_{CI_\alpha}} = \frac{g_C}{g_{N_c}}$ necrotic cancer cell agents. Recalling the discrete nature of agents, this amounts to spawning $\left\lfloor \frac{g_C}{g_{N_c}} \right\rfloor + Y$ agents corresponding to $\tilde{N}_c$, where $Y \sim \text{Bernoulli}\left(\{\frac{g_C}{g_{N_c}}\}\right)$.

The aforementioned conversion process provides a methodology for constructing ABMs from ODE systems with parameters calibrated to experimental data. Despite the non-spatial nature of ODEs, the agent-based framework easily accommodates the inclusion of spatial processes and interactions, such as diffusion and chemotaxis, by encoding them as agent-level properties and rules, should spatial structure be introduced.

3 Initial Conditions

3.1 Initial Conditions for Cells in the TS

The initial conditions for all cells in the TS are shown in Table 2 and are as in [35], except for naive macrophages. Justification for the choice of these values is in Appendix B.9.2.

C	N_c	D_0	D	T_8	T_{ex}
1.79×10^7	1.99×10^6	1.63×10^6	8.29×10^5	2.43×10^5	2.09×10^5
T_r	M_0	M_2	K_0	K	
2.12×10^5	5.58×10^5	1.23×10^6	3.06×10^5	5.20×10^6	

Table 2: TS initial condition cell densities for the model. All values are in cell/cm^3.

3.2 Initial Conditions for Cells in the TDLN

The initial conditions for all cells in the TDLN are shown in Table 3 and are as in [35], except for effector CD8+ T cells and effector Tregs. Justification for the choice of these values is in Appendix B.10.1 and Appendix B.10.2.

D^{LN}	T_0^8	T_A^8	T_0^r	T_A^r
1.05×10^7	1.20×10^7	1.30×10^6	9.95×10^4	7.85×10^5

Table 3: TDLN initial condition cell densities for the model. All values are in cell/cm^3.

3.3 Initial Conditions for Cytokines in the TS

We choose the TS immune checkpoint-associated component initial conditions to be as in Table 4, with justification for the choice of these values in Appendix B.3.

I_2	I_γ	I_α	I_β	I_{10}	I_{12}
2.73×10^{-12}	1.83×10^{-11}	5.75×10^{-11}	9.05×10^{-7}	6.22×10^{-11}	1.04×10^{-12}

Table 4: Cytokine initial conditions for the model. All values are in units of g/cm^3.

3.4 Initial Conditions for Immune Checkpoint-Associated Components in the TS

We choose the TS immune checkpoint-associated component initial conditions to be as in Table 5, with justification for the choice of these values in Appendix B.12.

$P_D^{T_8}$	P_D^K	P_L	Q^{T_8}	Q^K
6.70×10^8	2.87×10^9	3.55×10^{12}	5.06×10^5	2.17×10^6

Table 5: TS immune checkpoint-associated component initial conditions for the model. All values are in units of molec/cm^3.

3.5 Initial Conditions for Immune Checkpoint-Associated Components in the TDLN

We choose the TDLN immune checkpoint-associated component initial conditions to be as in Table 6, with justification for the choice of these values in Appendix B.13.

$P_D^{8\text{LN}}$	P_L^{LN}	$Q^{8\text{LN}}$
1.56×10^9	1.86×10^{11}	6.18×10^4

Table 6: TDLN immune checkpoint-associated component initial conditions for the model. All values are in units of molec/cm^3.

4 Results

In the absence of treatment, Figure 3 shows the time traces, up to 18 weeks, of the total cancer concentration, V, from the ODE model and ten ABM simulations, while Figure 4 shows the corresponding traces for all variables in the model.

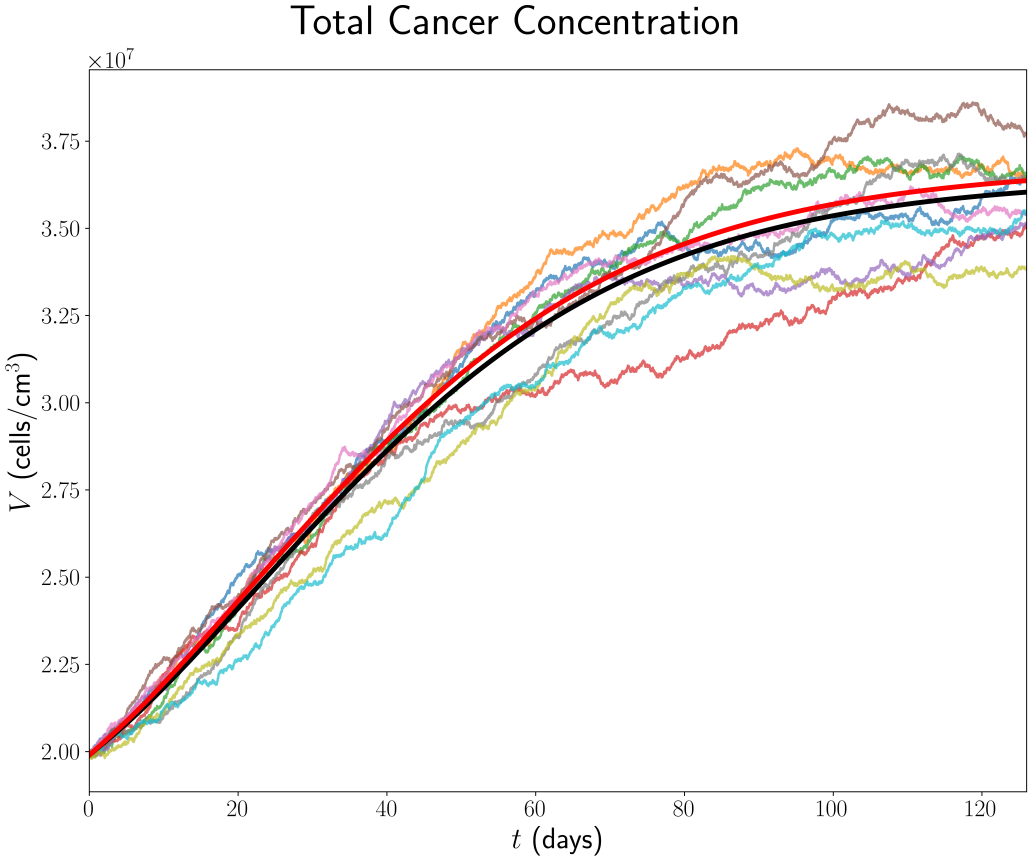

Figure 3: Time traces of V up to 18 weeks in the case of no treatment. The trajectory from the ODE model is shown in black, from the full model in [35] in red, from the full model in [35] in red, and the trajectories from ABM runs are coloured.

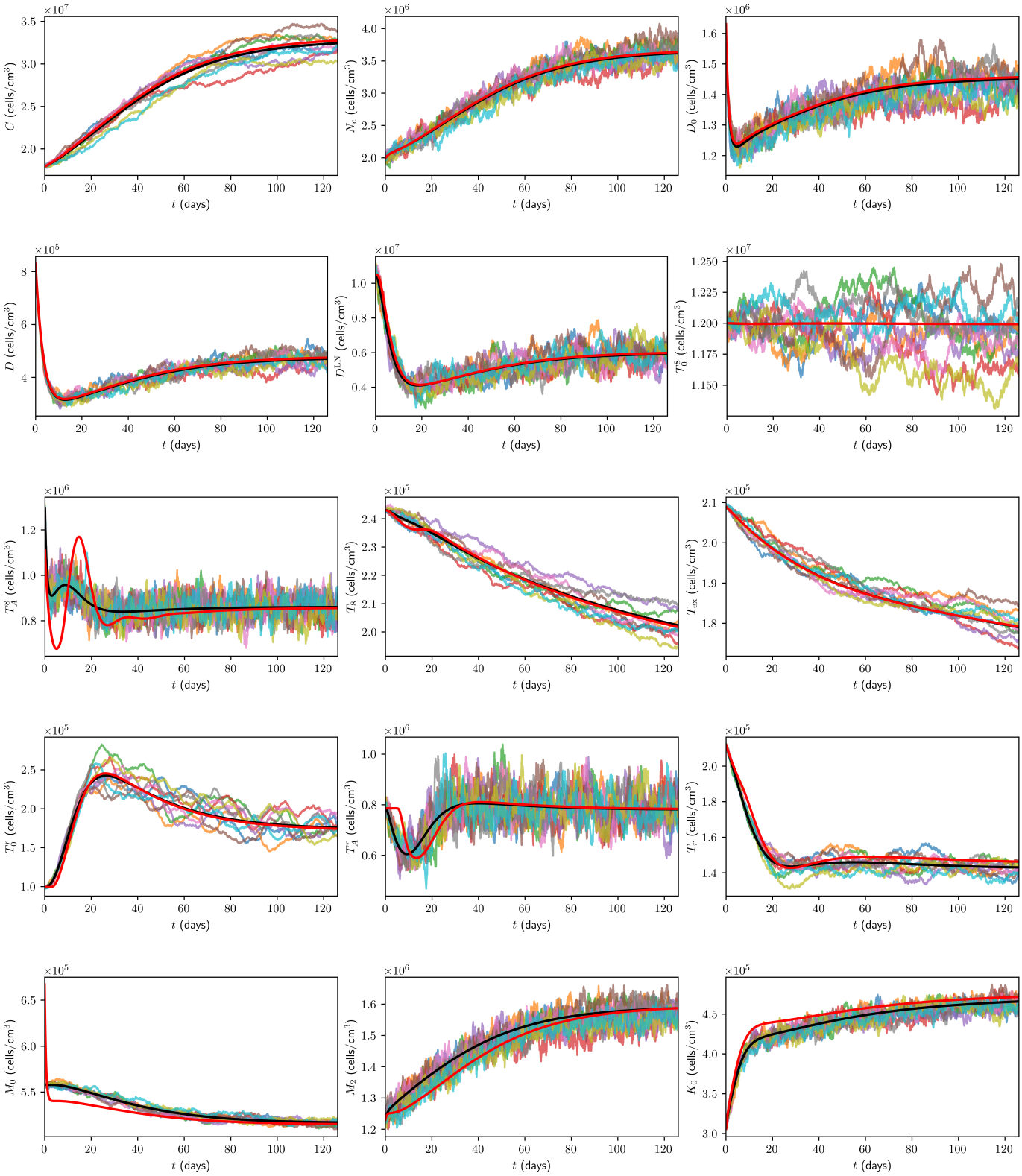
C (cells/cm^3)
N_c (cells/cm^3)
D_0 (cells/cm^3)
D (cells/cm^3)
D^{LN} (cells/cm^3)
T_0^8 (cells/cm^3)
T_A^8 (cells/cm^3)
T_8 (cells/cm^3)
T_{ex} (cells/cm^3)
T_0^T (cells/cm^3)
T_A^T (cells/cm^3)
T_T (cells/cm^3)
M_0 (cells/cm^3)
M_2 (cells/cm^3)
K_0 (cells/cm^3)
t (days)

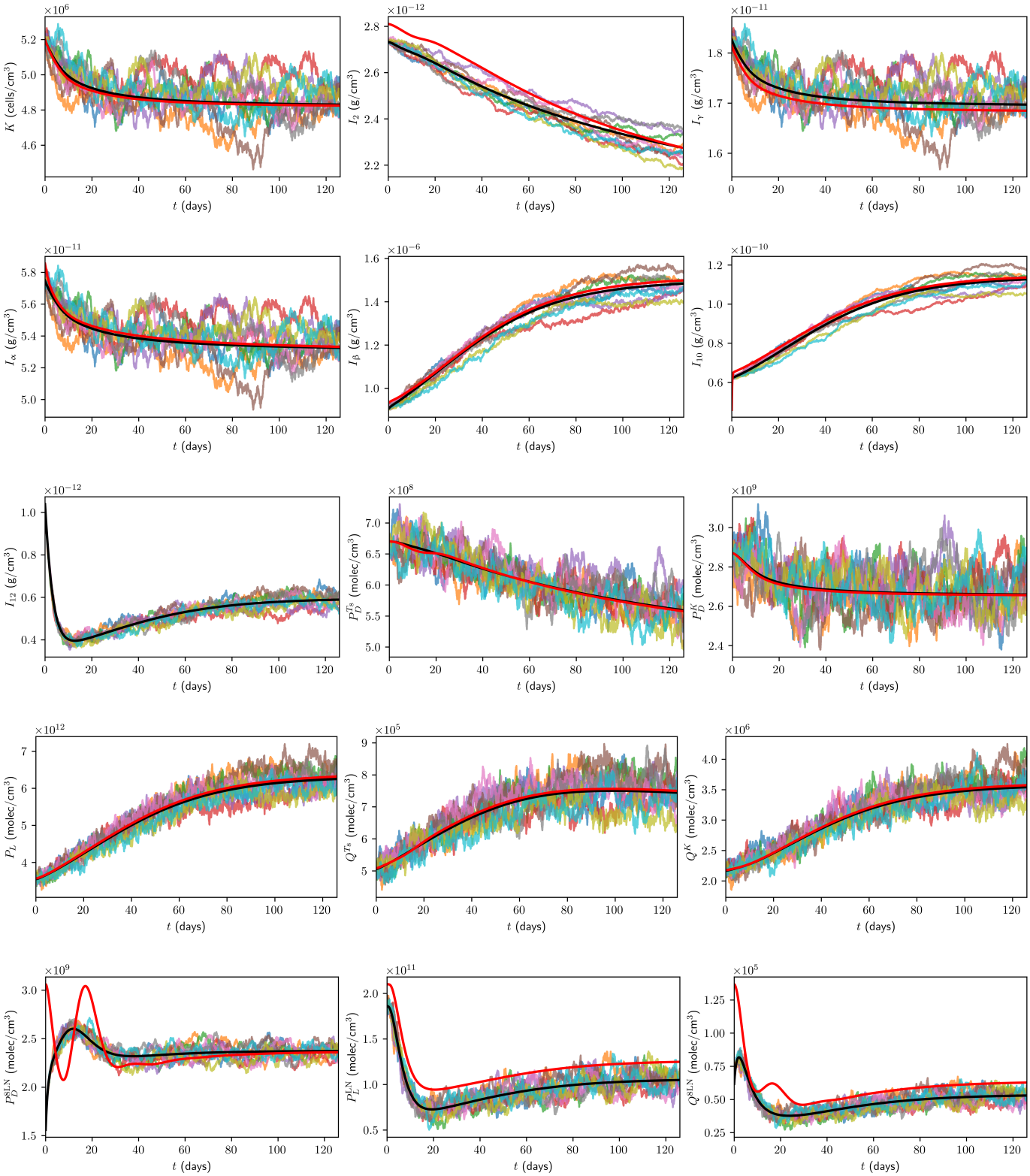

Figure 4: Time traces of variables in the model, in the case of no treatment, with the units of the variables as in Table 1. Trajectories from the ODE model are shown in black, from the full model in [35] in red, and the trajectories from ABM runs are coloured.

Furthermore, it is beneficial for us to compare the ODE and ABM models under neoadjuvant pembrolizumab therapy, which we assume commences at $t = 0$ days. As a benchmark for comparison, we consider treatment with 200 mg of pembrolizumab administered by intravenous infusion every 3

weeks, approved by the FDA for the first-line treatment of metastatic MSI-H/dMMR CRC [122]. Assuming a patient mass of $m = 80$ kg, these correspond to $\xi_j = 200$ mg, $t_j = 21(j-1)$, $n = 6$, $\xi_{\text{pembro}} = 2.5$ mg/kg, and $\eta_{\text{pembro}} = 3$ weeks. Time traces of V and all model variables, up to 18 weeks, from the ODE model and ten ABM simulations are shown in Figure 5 and Figure 6 in the case of this treatment, respectively.

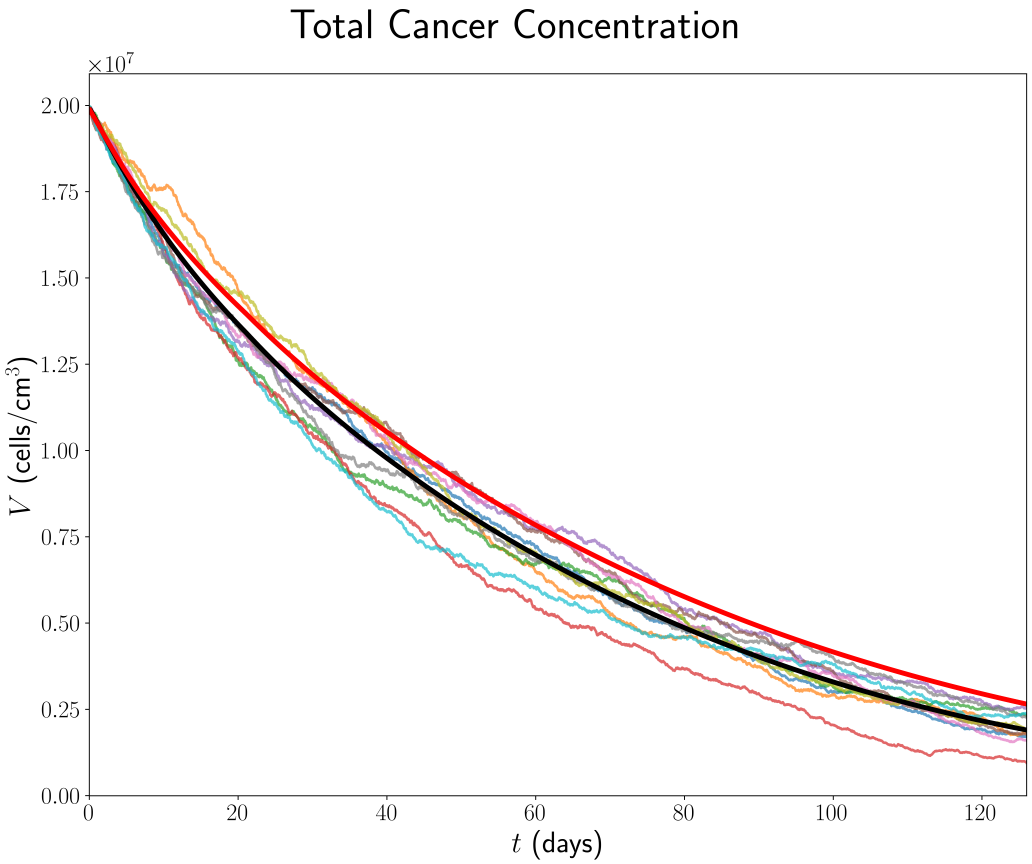

Figure 5: Time traces of V up to 18 weeks in the case of treatment with triweekly 200 mg pembrolizumab. The trajectory from the ODE model is shown in black, from the full model in [35] in red, and the trajectories from ABM runs are coloured.

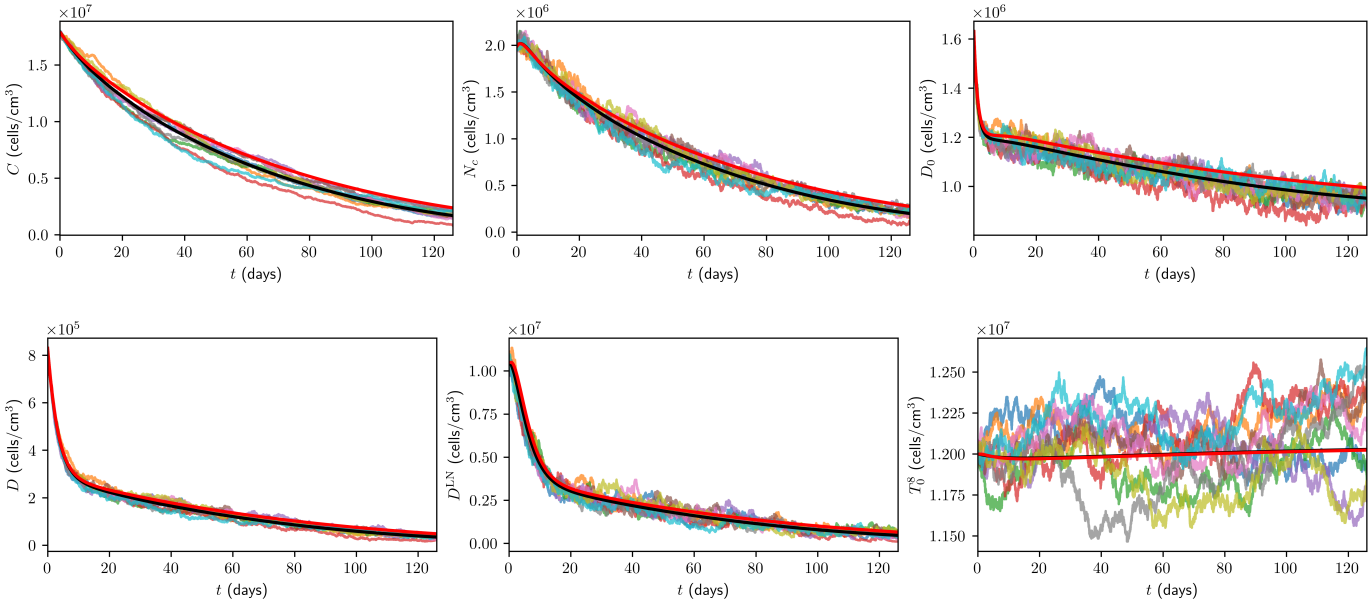

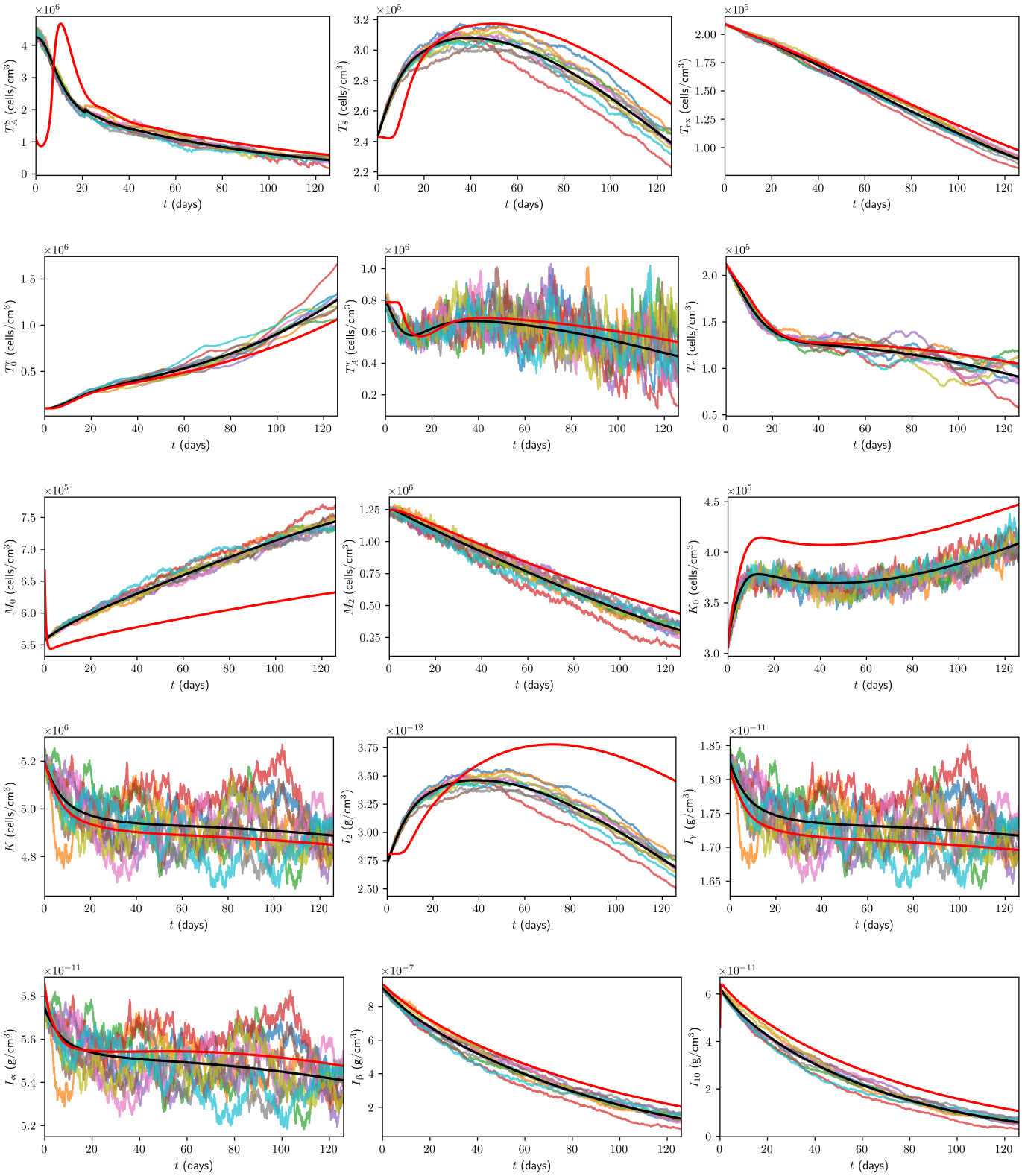
T_A^8 (cells/cm^3)
T_8 (cells/cm^3)
T_{ex} (cells/cm^3)
T_0^r (cells/cm^3)
T_A^r (cells/cm^3)
T_r (cells/cm^3)
M_0 (cells/cm^3)
M_2 (cells/cm^3)
K_0 (cells/cm^3)
K (cells/cm^3)
I_2 (g/cm^3)
I_γ (g/cm^3)
I_α (g/cm^3)
I_β (g/cm^3)
I_{10} (g/cm^3)
t (days)

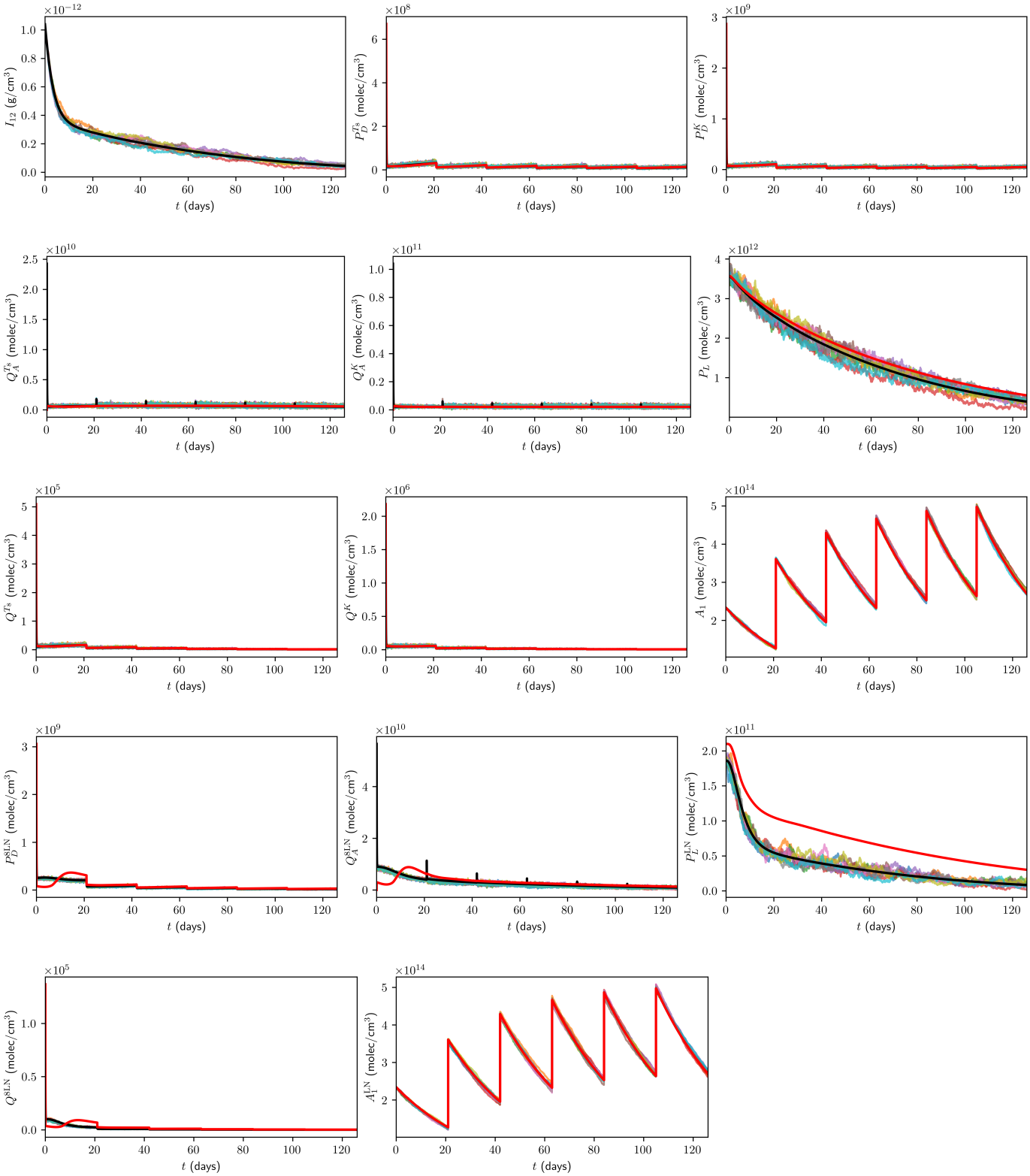

Figure 6: Time traces of variables in the model, in the case of treatment with triweekly 200 mg pembrolizumab, with the units of the variables as in Table 1. Trajectories from the ODE model are shown in black, from the full model in [35] in red, and the trajectories from ABM runs are coloured.

All ODE simulations of the minimal model were performed in MATLAB using the ode23 solver with the initial conditions stated in Section 3, whereas all DDE simulations of the full model were performed in MATLAB using the dde23 solver with the initial conditions stated in [35].

All ABM simulations were performed in Python 3.11 using the Mesa framework [123] with a constant time step of $\Delta t = 0.01$ day, and with group sizes as follows: for all $X \in \{T_A^8, T_A^r, M_0, I_2, I_\gamma, I_\alpha, I_\beta, I_{10}, I_{12}, Q_A^{T_8}, Q^{T_8}, Q_A^K, Q^K, Q_A^{8\text{LN}}, Q^{8\text{LN}}\}$, we set $g_X = 1$; for all $Y \in \{D_0, D, T_8, T_{\text{ex}}, T_r, M_2, K_0, K\}$, we set $g_Y = \frac{Y(0)V_{\text{TS}}}{2000}$; and for all $Z \in \{P_D^{T_8}, P_D^K, P_L\}$, we set $g_Z = \frac{Z(0)V_{\text{TS}}}{1000}$. Additionally $g_C = \frac{C(0)V_{\text{TS}}}{5000}$, $g_{N_C} = \frac{N_c(0)V_{\text{TS}}}{2000}$, $g_{A_1} = \frac{3\times10^{14}\times V_{\text{TS}}}{1000}$, $g_{D^{\text{LN}}} = \frac{D^{\text{LN}}(0)V_{\text{LN}}}{1000}$, $g_{T_0^8} = \frac{T_0^8(0)V_{\text{LN}}}{2000}$, $g_{T_0^r} = \frac{T_0^r(0)V_{\text{LN}}}{2000}$, $g_{P_D^{8\text{LN}}} = \frac{P_D^{8\text{LN}}(0)V_{\text{LN}}}{1000}$, $g_{P_L^{\text{LN}}} = \frac{P_L^{\text{LN}}(0)V_{\text{LN}}}{1000}$, and $g_{A_1^{\text{LN}}} = \frac{3\times10^{14}\times V_{\text{LN}}}{1000}$.

5 Discussion

Referencing Figure 3, Figure 4, Figure 5, and Figure 6, it is evident that the minimal model accurately reproduces the trajectories of the full model under both treatment and no-treatment conditions. In particular, the core dynamics are preserved, and we refer the reader to [35] for a detailed discussion on their biological implications and corresponding mechanistic insights. However, it is important to note that we observe some minor deviations, particularly after a couple of weeks, for variables related to the concentration of effector CD8+ T cells, naive macrophages, and immune checkpoint-associated components in the TDLN. These deviations are expected due to the nature and application of QSSA, which results in different initial conditions for these variables compared to the full and minimal models. Additionally, there are minor differences in the steady states and initial conditions of PD-L1 and PD-1/PD-L1 complex concentrations in the TDLN, which contribute to these deviations. This is more pronounced under treatment: PD-L1 in the TDLN originates solely from mature DCs, and pembrolizumab-driven tumour reduction decreases DAMP secretion from necrotic cancer cells, thereby reducing DC maturation and the influx of mature DCs to the TDLN. However, PD-L1 in the TDLN only influences the system through PD-1/PD-L1 complex formation, which appears through inhibition constants, rendering its absolute concentration, like that of several cytokines, less critical; accordingly, these deviations have minimal impact on the trajectories of other state variables, as observed.

In constructing a minimal model of pembrolizumab therapy in laMCRC, we removed variables corresponding to the concentration of DAMPs, CD4+ T cells and associated variables, and M1 macrophages, alongside their associated parameters. Additionally, with the application of QSSAs, further eliminated explicit dependencies on effector CD8+ T cells and Tregs in the TDLN, naive macrophages, IL-2, IFN-γ, TNF, TGF-β, IL-10, IL-12, and the PD-1/pembrolizumab complex on effector NK cells and effector CD8+ T cells in the TS and TDLN. This, in tandem with only retaining the most influential processes, results in an approximate 50% reduction in system dimensionality and a nearly 50% reduction in the number of parameters compared to the full model—representing a significant simplification while still accurately replicating model trajectories.

Consequently, replacing the integrals in the full model with point estimates is justified, suggesting that delay integro-differential equations may be unnecessarily complex for modelling the immunobiology of MSI-H/dMMR CRC, and that ODEs may be sufficient. We also hypothesise that the minimal model cannot be easily simplified or reduced without significantly affecting model trajectories, so that each component of the minimal model is functionally important, contributing meaningfully to the system's behaviour. However, verification of this requires methods such as sensitivity analysis [124–127] and identifiability analysis [128], which are beyond the scope of this work.

We observe that the ABM faithfully replicates the trajectories of the minimal ODE model under

both treatment and no-treatment conditions, considering Figure 3, Figure 4, Figure 5, and Figure 6, with the ABM exhibiting stochastic fluctuations around the ODE trajectories—as expected, since the ODE system represents the mean-field limit of the ABM. In particular, there is pronounced variation and stochasticity arising in model populations that undergo significant proliferation, especially cancer cells, NK cells, and T cells, since randomness can propagate, as proliferation events and bursty clonal expansion amplify and propagate randomness over time. This, in turn, induces fluctuations in the concentrations of secreted cytokines and in the expression of immune checkpoints, yielding correlated oscillations in IL-2, IFN-γ, TNF, TGF-β, IL-10, and tumoural PD-L1, which often directly influence the concentration of these cells, creating positive feedback loops, and reinforcing stochasticity. For example, IL-2 mediates effector CD8+ T cell expansion in the TS, whereas TGF-β inhibits effector CD8+ T cell and activated NK cell cytotoxicity against cancer cells. This results in amplified variability in effector and cancer cell concentrations in the ABM, manifesting as oscillations around the deterministic mean-field trajectories of the ODE system—nonetheless, maintaining close agreement with those governed by the deterministic model.

It should be noted that the models have several limitations, many of which exist for simplicity, but addressing these issues offers exciting avenues for future research.

- We ignored spatial effects in the model; however, their resolution can provide information about the distribution and clustering of different immune cell types in the TME and their clinical implications [129, 130]. Nevertheless, the ABM is naturally amenable to adding spatial mechanisms—including chemotaxis along cytokine gradients, explicit tumour and TDLN geometries, and the diffusion and advection of cells, cytokines, and proteins.

- We did not consider T cell avidity, the overall strength of a TCR-pMHC interaction, which governs whether a cancer cell will be successfully killed [131]. In particular, high-avidity T cells are necessary for lysing cancer cells and durable tumour eradication, while low-avidity T cells are ineffective and may inhibit high-avidity T cells [132, 133].

- We also did not consider the influence of cytokines in the TDLN for T cell activation and proliferation, which are important in influencing effector T cell differentiation [134, 135].

- The model does not explicitly account for additional anatomical compartments such as the spleen, nor does it directly model lymph node metastasis, which may impact the accuracy of systemic immune dynamics and tumour-specific responses; however, these features can be readily accommodated in ABMs.

In this work, we have constructed a minimal ODE model of neoadjuvant pembrolizumab therapy in laMCRC, and verified that it accurately reproduces the state-variable trajectories of larger, more comprehensive models, thereby preserving the most significant biological interactions and resultant tumour–immune dynamics. This, in turn, enhances interpretability and parameter identifiability and, combined with the model's self-contained nature and high extensibility, provides a robust foundation for future analysis and experimentation. Building on this foundation, we presented a practical and efficient workflow for translating differential-equation-based models into ABMs, enabling efficient and accurate calibration of model parameters and stochastic, individual-level representation while preserving consistency with the underlying deterministic system. Applying this framework to the minimal ODE model, we showed that the calibrated ABM faithfully reproduces its trajectories, thereby providing a principled basis for incorporating spatial effects, additional anatomical compartments, and patient-specific heterogeneity in future studies. Collectively, these advances establish a rigorous, flexible modelling paradigm that bridges parsimonious, calibrated deterministic dynamical systems with

calibrated, stochastic agent-based modelling—applicable to laMCRC and other biological systems—thereby accelerating treatment optimisation and personalisation and improving therapeutic outcomes.

6 CRediT Authorship Contribution Statement

Georgio Hawi: conceptualisation, data curation, formal analysis, funding acquisition, investigation, methodology, project administration, resources, software, validation, visualisation, writing — original draft, writing — review & editing.
Peter S. Kim: conceptualisation, formal analysis, funding acquisition, investigation, methodology, project administration, resources, supervision, validation, visualisation, writing — original draft, writing — review & editing.
Peter P. Lee: conceptualisation, formal analysis, investigation, methodology, project administration, resources, supervision, validation, visualisation, writing — original draft, writing — review & editing.

7 Declaration of Competing Interests

The authors declare that they have no known competing financial interests or personal relationships that could have appeared to influence the work reported in this paper.

8 Data Availability

All data and procedures are available within the manuscript and its Supporting Information file. Accompanying code is available at https://doi.org/10.5281/zenodo.16930420.

9 Acknowledgements

This work was supported by an Australian Government Research Training Program Scholarship. PSK gratefully acknowledges support from the Australian Research Council Discovery Project (DP230100485).

References

[1] Klimeck L, Heisser T, Hoffmeister M, Brenner H. Colorectal cancer: A health and economic problem. Best Practice & Research Clinical Gastroenterology. 2023 Oct;66:101839. Available from: https://doi.org/10.1016/j.bpg.2023.101839.

[2] Biller LH, Schrag D. Diagnosis and Treatment of Metastatic Colorectal Cancer: A Review. JAMA. 2021 Feb;325(7):669. Available from: https://doi.org/10.1001/jama.2021.0106.

[3] Siegel RL, Kratzer TB, Giaquinto AN, Sung H, Jemal A. Cancer statistics, 2025. CA: A Cancer Journal for Clinicians. 2025 Jan;75(1):10–45. Available from: https://doi.org/10.3322/caac.21871.

[4] Mulet-Margalef N, Linares J, Badia-Ramentol J, Jimeno M, Sanz Monte C, Manzano Mozo JL, et al. Challenges and Therapeutic Opportunities in the dMMR/MSI-H Colorectal Cancer Landscape. Cancers. 2023 Feb;15(4):1022. Available from: https://doi.org/10.3390/cancers15041022.

[5] Llosa NJ, Cruise M, Tam A, Wicks EC, Hechenbleikner EM, Taube JM, et al. The Vigorous Immune Microenvironment of Microsatellite Instable Colon Cancer Is Balanced by Multiple Counter-Inhibitory Checkpoints. Cancer Discovery. 2015 Jan;5(1):43–51. Available from: https://doi.org/10.1158/2159-8290.CD-14-0863.

[6] Giannakis M, Mu XJ, Shukla SA, Qian ZR, Cohen O, Nishihara R, et al. Genomic Correlates of Immune-Cell Infiltrates in Colorectal Carcinoma. Cell Reports. 2016 Apr;15(4):857–865. Available from: https://doi.org/10.1016/j.celrep.2016.03.075.

[7] Sinicrope FA, Foster NR, Thibodeau SN, Marsoni S, Monges G, Labianca R, et al. DNA Mismatch Repair Status and Colon Cancer Recurrence and Survival in Clinical Trials of 5-Fluorouracil-Based Adjuvant Therapy. JNCI Journal of the National Cancer Institute. 2011 May;103(11):863–875. Available from: https://doi.org/10.1093/jnci/djr153.

[8] Fan WX, Su F, Zhang Y, Zhang XL, Du YY, Gao YJ, et al. Oncological characteristics, treatments and prognostic outcomes in MMR-deficient colorectal cancer. Biomarker Research. 2024 Aug;12(1). Available from: https://doi.org/10.1186/s40364-024-00640-7.

[9] Gu J, Li Z, Zhou J, Sun Z, Bai C. Response prediction to oxaliplatin plus 5-fluorouracil chemotherapy in patients with colorectal cancer using a four-protein immunohistochemical model. Oncology Letters. 2019 Jun. Available from: https://doi.org/10.3892/ol.2019.10474.

[10] Shulman K, Barnett-Griness O, Friedman V, Greenson JK, Gruber SB, Lejbkowicz F, et al. Outcomes of Chemotherapy for Microsatellite Instable–High Metastatic Colorectal Cancers. JCO Precision Oncology. 2018 Nov;(2):1–10. Available from: https://doi.org/10.1200/PO.17.00253.

[11] Ciardiello D, Vitiello PP, Cardone C, Martini G, Troiani T, Martinelli E, et al. Immunotherapy of colorectal cancer: Challenges for therapeutic efficacy. Cancer Treatment Reviews. 2019 Jun;76:22–32. Available from: https://doi.org/10.1016/j.ctrv.2019.04.003.

[12] Topalian SL, Hodi FS, Brahmer JR, Gettinger SN, Smith DC, McDermott DF, et al. Safety, Activity, and Immune Correlates of Anti–PD-1 Antibody in Cancer. New England Journal of Medicine. 2012 Jun;366(26):2443–2454. Available from: https://doi.org/10.1056/NEJMoa1200690.

[13] Sarshekeh AM, Overman MJ, Kopetz S. Nivolumab in the Treatment of Microsatellite Instability High Metastatic Colorectal Cancer. Future Oncology. 2018 Feb;14(18):1869–1874. Available from: https://doi.org/10.2217/fon-2017-0696.

[14] Yaghoubi N, Soltani A, Ghazvini K, Hassanian SM, Hashemy SI. PD-1/ PD-L1 blockade as a novel treatment for colorectal cancer. Biomedicine & Pharmacotherapy. 2019 Feb;110:312–318. Available from: https://doi.org/10.1016/j.biopha.2018.11.105.

[15] Lin X, Kang K, Chen P, Zeng Z, Li G, Xiong W, et al. Regulatory mechanisms of PD-1/PD-L1 in cancers. Molecular Cancer. 2024 May;23(1). Available from: https://doi.org/10.1186/s12943-024-02023-w.

[16] Han Y, Liu D, Li L. PD-1/PD-L1 pathway: current researches in cancer. American journal of cancer research. 2020;10(3):727.

[17] Oliveira AF, Bretes L, Furtado I. Review of PD-1/PD-L1 Inhibitors in Metastatic dMMR/MSI-H Colorectal Cancer. Frontiers in Oncology. 2019 May;9. Available from: https://doi.org/10.3389/fonc.2019.00396.

[18] Lee J, Ahn E, Kissick HT, Ahmed R. Reinvigorating Exhausted T Cells by Blockade of the PD-1 Pathway. Forum on Immunopathological Diseases and Therapeutics. 2015;6(1–2):7–17. Available from: https://doi.org/10.1615/ForumImmunDisTher.2015014188.

[19] Zhang Y, Zhang Z. The history and advances in cancer immunotherapy: understanding the characteristics of tumor-infiltrating immune cells and their therapeutic implications. Cellular & Molecular Immunology. 2020 Jul;17(8):807–821. Available from: https://doi.org/10.1038/s41423-020-0488-6.

[20] André T, Shiu KK, Kim TW, Jensen BV, Jensen LH, Punt C, et al. Pembrolizumab in Microsatellite-Instability–High Advanced Colorectal Cancer. New England Journal of Medicine. 2020 Dec;383(23):2207–2218. Available from: https://doi.org/10.1056/NEJMoa2017699.

[21] Casak SJ, Marcus L, Fashoyin-Aje L, Mushti SL, Cheng J, Shen YL, et al. FDA Approval Summary: Pembrolizumab for the First-line Treatment of Patients with MSI-H/dMMR Advanced Unresectable or Metastatic Colorectal Carcinoma. Clinical Cancer Research. 2021 Apr;27(17):4680–4684. Available from: https://doi.org/10.1158/1078-0432.CCR-21-0557.

[22] Zhang X, Wu T, Cai X, Dong J, Xia C, Zhou Y, et al. Neoadjuvant Immunotherapy for MSI-H/dMMR Locally Advanced Colorectal Cancer: New Strategies and Unveiled Opportunities. Frontiers in Immunology. 2022 Mar;13. Available from: https://doi.org/10.3389/fimmu.2022.795972.

[23] Shiu KK, Jiang Y, Saunders M, Seligmann JF, Iveson T, Wilson RH, et al. NEOPRISM-CRC: Neoadjuvant pembrolizumab stratified to tumour mutation burden for high risk stage 2 or stage 3 deficient-MMR/MSI-high colorectal cancer. Journal of Clinical Oncology. 2024 Jun;42(17_suppl):LBA3504–LBA3504. Available from: https://doi.org/10.1200/JCO.2024.42.17_suppl.LBA3504.

[24] Ludford K, Ho WJ, Thomas JV, Raghav KPS, Murphy MB, Fleming ND, et al. Neoadjuvant Pembrolizumab in Localized Microsatellite Instability High/Deficient Mismatch Repair Solid Tumors. Journal of Clinical Oncology. 2023 Apr;41(12):2181–2190. Available from: https://doi.org/10.1200/JCO.22.01351.

[25] LaPelusa M, Qiao W, Iorgulescu B, San Lucas F, Patel K, Bhamidipati D, et al. Long-Term Efficacy of Pembrolizumab and the Clinical Utility of ctDNA in Locally Advanced dMMR/MSI-H Solid Tumors. Nature Communications. 2025 May;16(1). Available from: https://doi.org/10.1038/s41467-025-59615-3.

[26] Kirshtein A, Akbarinejad S, Hao W, Le T, Su S, Aronow RA, et al. Data Driven Mathematical Model of Colon Cancer Progression. Journal of Clinical Medicine. 2020 Dec;9(12):3947. Available from: https://doi.org/10.3390/jcm9123947.

[27] Budithi A, Su S, Kirshtein A, Shahriyari L. Data Driven Mathematical Model of FOLFIRI Treatment for Colon Cancer. Cancers. 2021 May;13(11):2632. Available from: https://doi.org/10.3390/cancers13112632.

[28] Bozkurt F, Yousef A, Bilgil H, Baleanu D. A mathematical model with piecewise constant arguments of colorectal cancer with chemo-immunotherapy. Chaos, Solitons & Fractals. 2023 Mar;168:113207. Available from: https://doi.org/10.1016/j.chaos.2023.113207.

[29] dePillis L. Mathematical Model of Colorectal Cancer with Monoclonal Antibody Treatments. British Journal of Medicine and Medical Research. 2014 Jan;4(16):3101–3131. Available from: https://doi.org/10.9734/BJMMR/2014/8393.

[30] Lai X, Friedman A. Combination therapy of cancer with cancer vaccine and immune checkpoint inhibitors: A mathematical model. PLOS ONE. 2017 May;12(5):e0178479. Available from: https://doi.org/10.1371/journal.pone.0178479.

[31] Lai X, Friedman A. How to schedule VEGF and PD-1 inhibitors in combination cancer therapy? BMC Systems Biology. 2019 Mar;13(1). Available from: https://doi.org/10.1186/s12918-019-0706-y.

[32] Siewe N, Friedman A. TGF-β inhibition can overcome cancer primary resistance to PD-1 blockade: A mathematical model. PLOS ONE. 2021 Jun;16(6):e0252620. Available from: https://doi.org/10.1371/journal.pone.0252620.

[33] Siewe N, Friedman A. Cancer therapy with immune checkpoint inhibitor and CSF-1 blockade: A mathematical model. Journal of Theoretical Biology. 2023 Jan;556:111297. Available from: https://doi.org/10.1016/j.jtbi.2022.111297.

[34] Liao KL, Bai XF, Friedman A. IL-27 in combination with anti-PD-1 can be anti-cancer or pro-cancer. Journal of Theoretical Biology. 2024 Feb;579:111704. Available from: https://doi.org/10.1016/j.jtbi.2023.111704.

[35] Hawi G, Kim PS, Lee PP. Optimisation of neoadjuvant pembrolizumab therapy for locally advanced MSI-H/dMMR colorectal cancer using data-driven delay integro-differential equations. Journal of Theoretical Biology. 2025 Aug:112231. Available from: https://doi.org/10.1016/j.jtbi.2025.112231.

[36] Zhang XY, Trame M, Lesko L, Schmidt S. Sobol Sensitivity Analysis: A Tool to Guide the Development and Evaluation of Systems Pharmacology Models. CPT: Pharmacometrics &amp: Systems Pharmacology. 2015 Feb;4(2):69-79. Available from: https://doi.org/10.1002/psp4.6.

[37] Metzcar J, Wang Y, Heiland R, Macklin P. A Review of Cell-Based Computational Modeling in Cancer Biology. JCO Clinical Cancer Informatics. 2019 Dec;(3):1–13. Available from: https://doi.org/10.1200/CCI.18.00069.

[38] West J, Robertson-Tessi M, Anderson ARA. Agent-based methods facilitate integrative science in cancer. Trends in Cell Biology. 2023 Apr;33(4):300–311. Available from: https://doi.org/10.1016/j.tcb.2022.10.006.

[39] Irurzun-Arana I, Rackauckas C, McDonald TO, Trocóniz IF. Beyond Deterministic Models in Drug Discovery and Development. Trends in Pharmacological Sciences. 2020 Nov;41(11):882–895. Available from: https://doi.org/10.1016/j.tips.2020.09.005.

[40] Kather JN, Poleszczuk J, Suarez-Carmona M, Krisam J, Charoentong P, Valous NA, et al. In Silico Modeling of Immunotherapy and Stroma-Targeting Therapies in Human Colorectal Cancer. Cancer Research. 2017 Nov;77(22):6442–6452. Available from: https://doi.org/10.1158/0008-5472.CAN-17-2006.

[41] Kather JN, Charoentong P, Suarez-Carmona M, Herpel E, Klupp F, Ulrich A, et al. High-Throughput Screening of Combinatorial Immunotherapies with Patient-Specific In Silico Models of Metastatic Colorectal Cancer. Cancer Research. 2018 Sep;78(17):5155–5163. Available from: https://doi.org/10.1158/0008-5472.CAN-18-1126.

[42] Gong C, Milberg O, Wang B, Vicini P, Narwal R, Roskos L, et al. A computational multiscale agent-based model for simulating spatio-temporal tumour immune response to PD1 and PDL1 inhibition. Journal of The Royal Society Interface. 2017 Sep;14(134):20170320. Available from: https://doi.org/10.1098/rsif.2017.0320.

[43] Wang Y, Zhu T, Shi Q, Zhu G, Zhu S, Hou F. Tumor-draining lymph nodes: opportunities, challenges, and future directions in colorectal cancer immunotherapy. Journal for ImmunoTherapy of Cancer. 2024 Jan;12(1):e008026. Available from: https://doi.org/10.1136/jitc-2023-008026.

[44] Raskov H, Orhan A, Christensen JP, Gögenur I. Cytotoxic CD8+ T cells in cancer and cancer immunotherapy. British Journal of Cancer. 2020 Sep;124(2):359–367. Available from: https://doi.org/10.1038/s41416-020-01048-4.

[45] Zhang C, Hu Y, Shi C. Targeting Natural Killer Cells for Tumor Immunotherapy. Frontiers in Immunology. 2020 Feb;11. Available from: https://doi.org/10.3389/fimmu.2020.00060.

[46] Josephs SF, Ichim TE, Prince SM, Kesari S, Marincola FM, Escobedo AR, et al. Unleashing endogenous TNF-alpha as a cancer immunotherapeutic. Journal of Translational Medicine. 2018 Aug;16(1). Available from: https://doi.org/10.1186/s12967-018-1611-7.

[47] Wang X, Lin Y. Tumor necrosis factor and cancer, buddies or foes? Acta Pharmacologica Sinica. 2008 Nov;29(11):1275–1288. Available from: https://doi.org/10.1111/j.1745-7254.2008.00889.x.

[48] Jorgovanovic D, Song M, Wang L, Zhang Y. Roles of IFN-γ in tumor progression and regression: a review. Biomarker Research. 2020 Sep;8(1). Available from: https://doi.org/10.1186/s40364-020-00228-x.

[49] Castro F, Cardoso AP, Gonçalves RM, Serre K, Oliveira MJ. Interferon-Gamma at the Crossroads of Tumor Immune Surveillance or Evasion. Frontiers in Immunology. 2018 May;9. Available from: https://doi.org/10.3389/fimmu.2018.00847.

[50] Thomas DA, Massagué J. TGF-β directly targets cytotoxic T cell functions during tumor evasion of immune surveillance. Cancer Cell. 2005 Nov;8(5):369–380. Available from: https://doi.org/10.1016/j.ccr.2005.10.012.

[51] Juneja VR, McGuire KA, Manguso RT, LaFleur MW, Collins N, Haining WN, et al. PD-L1 on tumor cells is sufficient for immune evasion in immunogenic tumors and inhibits CD8 T cell cytotoxicity. Journal of Experimental Medicine. 2017 Mar;214(4):895–904. Available from: https://doi.org/10.1084/jem.20160801.

[52] Azuma T, Yao S, Zhu G, Flies AS, Flies SJ, Chen L. B7-H1 is a ubiquitous antiapoptotic receptor on cancer cells. Blood. 2008 Apr;111(7):3635–3643. Available from: https://doi.org/10.1182/blood-2007-11-123141.

[53] Regis S, Dondero A, Caliendo F, Bottino C, Castriconi R. NK Cell Function Regulation by TGF-β-Induced Epigenetic Mechanisms. Frontiers in Immunology. 2020 Feb;11. Available from: https://doi.org/10.3389/fimmu.2020.00311.

[54] Batlle E, Massagué J. Transforming Growth Factor-β Signaling in Immunity and Cancer. Immunity. 2019 Apr;50(4):924–940. Available from: https://doi.org/10.1016/j.immuni.2019.03.024.

[55] Hsu J, Hodgins JJ, Marathe M, Nicolai CJ, Bourgeois-Daigneault MC, Trevino TN, et al. Contribution of NK cells to immunotherapy mediated by PD-1/PD-L1 blockade. Journal of Clinical Investigation. 2018 Sep;128(10):4654–4668. Available from: https://doi.org/10.1172/JCI99317.

[56] Quatrini L, Mariotti FR, Munari E, Tumino N, Vacca P, Moretta L. The Immune Checkpoint PD-1 in Natural Killer Cells: Expression, Function and Targeting in Tumour Immunotherapy. Cancers. 2020 Nov;12(11):3285. Available from: https://doi.org/10.3390/cancers12113285.

[57] Liu Y, Cheng Y, Xu Y, Wang Z, Du X, Li C, et al. Increased expression of programmed cell death protein 1 on NK cells inhibits NK-cell-mediated anti-tumor function and indicates poor prognosis in digestive cancers. Oncogene. 2017 Jul;36(44):6143–6153. Available from: https://doi.org/10.1038/onc.2017.209.

[58] Del Prete A, Salvi V, Soriani A, Laffranchi M, Sozio F, Bosisio D, et al. Dendritic cell subsets in cancer immunity and tumor antigen sensing. Cellular & Molecular Immunology. 2023 Mar;20(5):432–447. Available from: https://doi.org/10.1038/s41423-023-00990-6.

[59] Morandi B, Mortara L, Chiossone L, Accolla RS, Mingari MC, Moretta L, et al. Dendritic Cell Editing by Activated Natural Killer Cells Results in a More Protective Cancer-Specific Immune Response. PLoS ONE. 2012 Jun;7(6):e39170. Available from: https://doi.org/10.1371/journal.pone.0039170.

[60] Vivier E, Tomasello E, Baratin M, Walzer T, Ugolini S. Functions of natural killer cells. Nature Immunology. 2008 Apr;9(5):503–510. Available from: https://doi.org/10.1038/ni1582.

[61] Castriconi R, Cantoni C, Della Chiesa M, Vitale M, Marcenaro E, Conte R, et al. Transforming growth factor β1 inhibits expression of NKp30 and NKG2D receptors: Consequences for the NK-mediated killing of dendritic cells. Proceedings of the National Academy of Sciences. 2003 Mar;100(7):4120–4125. Available from: https://doi.org/10.1073/pnas.0730640100.

[62] Ruhland MK, Roberts EW, Cai E, Mujal AM, Marchuk K, Beppler C, et al. Visualizing Synaptic Transfer of Tumor Antigens among Dendritic Cells. Cancer Cell. 2020 Jun;37(6):786-99.e5. Available from: https://doi.org/10.1016/j.ccell.2020.05.002.

[63] Choi G, Kim BS, Park YJ, Shim I, Chung Y. Clonal Expansion of Allergen-specific CD4+ T Cell in the Lung in the Absence of Lymph Nodes. Immune Network. 2017;17(3):163. Available from: https://doi.org/10.4110/in.2017.17.3.163.

[64] Tadokoro CE, Shakhar G, Shen S, Ding Y, Lino AC, Maraver A, et al. Regulatory T cells inhibit stable contacts between CD4+ T cells and dendritic cells in vivo. The Journal of Experimental Medicine. 2006 Mar;203(3):505–511. Available from: https://doi.org/10.1084/jem.20050783.

[65] Chen BJ, Zhao JW, Zhang DH, Zheng AH, Wu GQ. Immunotherapy of Cancer by Targeting Regulatory T cells. International Immunopharmacology. 2022 Mar;104:108469. Available from: https://doi.org/10.1016/j.intimp.2021.108469.

[66] Li C, Jiang P, Wei S, Xu X, Wang J. Regulatory T cells in tumor microenvironment: new mechanisms, potential therapeutic strategies and future prospects. Molecular Cancer. 2020 Jul;19(1). Available from: https://doi.org/10.1186/s12943-020-01234-1.

[67] Sakaguchi S, Yamaguchi T, Nomura T, Ono M. Regulatory T Cells and Immune Tolerance. Cell. 2008 May;133(5):775–787. Available from: https://doi.org/10.1016/j.cell.2008.05.009.

[68] Brunner-Weinzierl MC, Rudd CE. CTLA-4 and PD-1 Control of T-Cell Motility and Migration: Implications for Tumor Immunotherapy. Frontiers in Immunology. 2018 Nov;9. Available from: https://doi.org/10.3389/fimmu.2018.02737.

[69] Mizuno R, Sugiura D, Shimizu K, Maruhashi T, Watada M, Okazaki Im, et al. PD-1 Primarily Targets TCR Signal in the Inhibition of Functional T Cell Activation. Frontiers in Immunology. 2019 Mar;10. Available from: https://doi.org/10.3389/fimmu.2019.00630.

[70] Chen RY, Zhu Y, Shen YY, Xu QY, Tang HY, Cui NX, et al. The role of PD-1 signaling in health and immune-related diseases. Frontiers in Immunology. 2023 May;14. Available from: https://doi.org/10.3389/fimmu.2023.1163633.

[71] Peng Q, Qiu X, Zhang Z, Zhang S, Zhang Y, Liang Y, et al. PD-L1 on dendritic cells attenuates T cell activation and regulates response to immune checkpoint blockade. Nature Communications. 2020 Sep;11(1). Available from: https://doi.org/10.1038/s41467-020-18570-x.

[72] Arasanz H, Gato-Cañas M, Zuazo M, Ibañez-Vea M, Breckpot K, Kochan G, et al. PD1 signal transduction pathways in T cells. Oncotarget. 2017 Apr;8(31):51936–51945. Available from: https://doi.org/10.18632/oncotarget.17232.

[73] Harris NL, Watt V, Ronchese F, Le Gros G. Differential T Cell Function and Fate in Lymph Node and Nonlymphoid Tissues. The Journal of Experimental Medicine. 2002 Feb;195(3):317–326. Available from: https://doi.org/10.1084/jem.20011558.

[74] Catron DM, Rusch LK, Hataye J, Itano AA, Jenkins MK. CD4+ T cells that enter the draining lymph nodes after antigen injection participate in the primary response and become central–memory cells. The Journal of Experimental Medicine. 2006 Mar;203(4):1045–1054. Available from: https://doi.org/10.1084/jem.20051954.

[75] Riley JL. PD-1 signaling in primary T cells. Immunological Reviews. 2009 Apr;229(1):114–125. Available from: https://doi.org/10.1111/j.1600-065X.2009.00767.x.

[76] Buchbinder EI, Desai A. CTLA-4 and PD-1 Pathways: Similarities, Differences, and Implications of Their Inhibition. American Journal of Clinical Oncology. 2016 Feb;39(1):98–106. Available from: https://doi.org/10.1097/COC.0000000000000239.

[77] Rosenberg SA. IL-2: The First Effective Immunotherapy for Human Cancer. The Journal of Immunology. 2014 Jun;192(12):5451–5458. Available from: https://doi.org/10.4049/jimmunol.1490019.

[78] Oft M. Immune regulation and cytotoxic T cell activation of IL-10 agonists – Preclinical and clinical experience. Seminars in Immunology. 2019 Aug;44:101325. Available from: https://doi.org/10.1016/j.smim.2019.101325.

[79] Qiu H, Hu X, Gao L, Chen L, Chen J, Yuan J, et al. Interleukin 10 enhanced CD8+ T cell activity and reduced CD8+ T cell apoptosis in patients with diffuse large B cell lymphoma. Experimental Cell Research. 2017 Nov;360(2):146–152. Available from: https://doi.org/10.1016/j.yexcr.2017.08.036.

[80] Blank CU, Haining WN, Held W, Hogan PG, Kallies A, Lugli E, et al. Defining 'T cell exhaustion'. Nature Reviews Immunology. 2019 Sep;19(11):665–674. Available from: https://doi.org/10.1038/s41577-019-0221-9.

[81] Lee KA, Shin KS, Kim GY, Song YC, Bae EA, Kim IK, et al. Characterization of age-associated exhausted CD8+ T cells defined by increased expression of Tim-3 and PD-1. Aging Cell. 2016 Jan;15(2):291–300. Available from: https://doi.org/10.1111/acel.12435.

[82] Shive CL, Freeman ML, Younes S, Kowal CM, Canaday DH, Rodriguez B, et al. Markers of T Cell Exhaustion and Senescence and Their Relationship to Plasma TGF-β Levels in Treated HIV+ Immune Non-responders. Frontiers in Immunology. 2021 Mar;12. Available from: https://doi.org/10.3389/fimmu.2021.638010.

[83] Pauken KE, Wherry EJ. Overcoming T cell exhaustion in infection and cancer. Trends in Immunology. 2015 Apr;36(4):265–276. Available from: https://doi.org/10.1016/j.it.2015.02.008.

[84] De Boer RJ, Perelson AS. Towards a general function describing T cell proliferation. Journal of Theoretical Biology. 1995 Aug;175(4):567–576. Available from: https://doi.org/10.1006/jtbi.1995.0165.

[85] Kroner A, Greenhalgh AD, Zarruk JG, Passos dos Santos R, Gaestel M, David S. TNF and Increased Intracellular Iron Alter Macrophage Polarization to a Detrimental M1 Phenotype in the Injured Spinal Cord. Neuron. 2014 Sep;83(5):1098–1116. Available from: https://doi.org/10.1016/j.neuron.2014.07.027.

[86] Kratochvill F, Neale G, Haverkamp JM, Van de Velde LA, Smith AM, Kawauchi D, et al. TNF Counterbalances the Emergence of M2 Tumor Macrophages. Cell Reports. 2015 Sep;12(11):1902–1914. Available from: https://doi.org/10.1016/j.celrep.2015.08.033.

[87] Nathan CF, Murray HW, Wiebe ME, Rubin BY. Identification of interferon-gamma as the lymphokine that activates human macrophage oxidative metabolism and antimicrobial activity. The Journal of experimental medicine. 1983 Sep;158(3):670–689. Available from: https://doi.org/10.1084/jem.158.3.670.

[88] Ivashkiv LB. IFNγ: signalling, epigenetics and roles in immunity, metabolism, disease and cancer immunotherapy. Nature Reviews Immunology. 2018 Jun;18(9):545–558. Available from: https://doi.org/10.1038/s41577-018-0029-z.

[89] Ambade A, Satishchandran A, Saha B, Gyongyosi B, Lowe P, Kodys K, et al. Hepatocellular carcinoma is accelerated by NASH involving M2 macrophage polarization mediated by hif-1αinduced IL-10. OncoImmunology. 2016 Sep;5(10):e1221557. Available from: https://doi.org/10.1080/2162402X.2016.1221557.

[90] Chen Y, Song Y, Du W, Gong L, Chang H, Zou Z. Tumor-associated macrophages: an accomplice in solid tumor progression. Journal of Biomedical Science. 2019 Oct;26(1). Available from: https://doi.org/10.1186/s12929-019-0568-z.

[91] Zhang F, Wang H, Wang X, Jiang G, Liu H, Zhang G, et al. TGF-β induces M2-like macrophage polarization via SNAIL-mediated suppression of a pro-inflammatory phenotype. Oncotarget. 2016 Jul;7(32):52294–52306. Available from: https://doi.org/10.18632/oncotarget.10561.

[92] Konjević GM, Vuletić AM, Mirjačić Martinović KM, Larsen AK, Jurišić VB. The role of cytokines in the regulation of NK cells in the tumor environment. Cytokine. 2019 May;117:30–40. Available from: https://doi.org/10.1016/j.cyto.2019.02.001.

[93] Widowati W, K Jasaputra D, B Sumitro S, A Widodo M, Mozef T, Rizal R, et al. Effect of interleukins (IL-2, IL-15, IL-18) on receptors activation and cytotoxic activity of natural killer cells in breast cancer cell. African Health Sciences. 2020 Jul;20(2):822–832. Available from: https://doi.org/10.4314/ahs.v20i2.36.

[94] Viel S, Marçais A, Guimaraes FSF, Loftus R, Rabilloud J, Grau M, et al. TGF-β inhibits the activation and functions of NK cells by repressing the mTOR pathway. Science Signaling. 2016 Feb;9(415). Available from: https://doi.org/10.1126/scisignal.aad1884.

[95] Kish DD, Gorbachev AV, Fairchild RL. CD8+ T cells produce IL-2, which is required for CD4+CD25+ T cell regulation of effector CD8+ T cell development for contact hypersensitivity responses. Journal of Leukocyte Biology. 2005 Jul;78(3):725–735. Available from: https://doi.org/10.1189/jlb.0205069.

[96] D'Souza WN, Lefranccois L. Frontline: An in-depth evaluation of the production of IL-2 by antigen-specific CD8 T cells in vivo. European Journal of Immunology. 2004 Oct;34(11):2977–2985. Available from: https://doi.org/10.1002/eji.200425485.

[97] Cui F, Qu D, Sun R, Zhang M, Nan K. NK cell-produced IFN-γ regulates cell growth and apoptosis of colorectal cancer by regulating IL-15. Experimental and Therapeutic Medicine. 2019 Dec. Available from: https://doi.org/10.3892/etm.2019.8343.

[98] Hoekstra ME, Vijver SV, Schumacher TN. Modulation of the tumor micro-environment by CD8+ T cell-derived cytokines. Current Opinion in Immunology. 2021 Apr;69:65–71. Available from: https://doi.org/10.1016/j.coi.2021.03.016.

[99] Mehta AK, Gracias DT, Croft M. TNF activity and T cells. Cytokine. 2018 Jan;101:14–18. Available from: https://doi.org/10.1016/j.cyto.2016.08.003.

[100] Fauriat C, Long EO, Ljunggren HG, Bryceson YT. Regulation of human NK-cell cytokine and chemokine production by target cell recognition. Blood. 2010 Mar;115(11):2167–2176. Available from: https://doi.org/10.1182/blood-2009-08-238469.

[101] Wang R, Jaw JJ, Stutzman NC, Zou Z, Sun PD. Natural killer cell-produced IFN-γ and TNF-α induce target cell cytolysis through up-regulation of ICAM-1. Journal of Leukocyte Biology. 2011 Nov;91(2):299–309. Available from: https://doi.org/10.1189/jlb.0611308.

[102] Massagué J. TGFβ in Cancer. Cell. 2008 Jul;134(2):215–230. Available from: https://doi.org/10.1016/j.cell.2008.07.001.

[103] Nuñez SY, Ziblat A, Secchiari F, Torres NI, Sierra JM, Raffo Iraolagoitia XL, et al. Human M2 Macrophages Limit NK Cell Effector Functions through Secretion of TGF-β and Engagement of CD85j. The Journal of Immunology. 2018 Feb;200(3):1008–1015. Available from: https://doi.org/10.4049/jimmunol.1700737.

[104] Itakura E, Huang RR, Wen DR, Paul E, Wünsch PH, Cochran AJ. IL-10 expression by primary tumor cells correlates with melanoma progression from radial to vertical growth phase and development of metastatic competence. Modern Pathology. 2011 Jun;24(6):801–809. Available from: https://doi.org/10.1038/modpathol.2011.5.

[105] Krüger-Krasagakes S, Krasagakis K, Garbe C, Schmitt E, Hüls C, Blankenstein T, et al. Expression of interleukin 10 in human melanoma. British Journal of Cancer. 1994 Dec;70(6):1182–1185. Available from: https://doi.org/10.1038/bjc.1994.469.

[106] Heufler C, Koch F, Stanzl U, Topar G, Wysocka M, Trinchieri G, et al. Interleukin-12 is produced by dendritic cells and mediates T helper 1 development as well as interferon-γ production by T helper 1 cells. European Journal of Immunology. 1996 Apr;26(3):659–668. Available from: https://doi.org/10.1002/eji.1830260323.

[107] Saito H, Kuroda H, Matsunaga T, Osaki T, Ikeguchi M. Increased PD-1 expression on CD4+ and CD8+ T cells is involved in immune evasion in gastric cancer. Journal of Surgical Oncology. 2012 Nov;107(5):517–522. Available from: https://doi.org/10.1002/jso.23281.

[108] Wu X, Zhang H, Xing Q, Cui J, Li J, Li Y, et al. PD-1+ CD8+ T cells are exhausted in tumours and functional in draining lymph nodes of colorectal cancer patients. British Journal of Cancer. 2014 Aug;111(7):1391–1399. Available from: https://doi.org/10.1038/bjc.2014.416.

[109] Jiang Y, Li Y, Zhu B. T-cell exhaustion in the tumor microenvironment. Cell Death & Disease. 2015 Jun;6(6):e1792–e1792. Available from: https://doi.org/10.1038/cddis.2015.162.

[110] Al-Mterin MA, Murshed K, Elkord E. PD-1 expression, among other immune checkpoints, on tumor-infiltrating NK and NKT cells is associated with longer disease-free survival in treatment-naïve CRC patients. Cancer Immunology, Immunotherapy. 2022 Nov;72(6):1933–1939. Available from: https://doi.org/10.1007/s00262-022-03337-8.

[111] Lin DYw, Tanaka Y, Iwasaki M, Gittis AG, Su HP, Mikami B, et al. The PD-1/PD-L1 complex resembles the antigen-binding Fv domains of antibodies and T cell receptors. Proceedings of the National Academy of Sciences. 2008 Feb;105(8):3011–3016. Available from: https://doi.org/10.1073/pnas.0712278105.

[112] Na Z, Yeo SP, Bharath SR, Bowler MW, Balıkçı E, Wang CI, et al. Structural basis for blocking PD-1-mediated immune suppression by therapeutic antibody pembrolizumab. Cell Research. 2016 Jun;27(1):147–150. Available from: https://doi.org/10.1038/cr.2016.77.

[113] Tan S, Zhang CWH, Gao GF. Seeing is believing: anti-PD-1/PD-L1 monoclonal antibodies in action for checkpoint blockade tumor immunotherapy. Signal Transduction and Targeted Therapy. 2016 Nov;1(1). Available from: https://doi.org/10.1038/sigtrans.2016.29.

[114] Wang S, Khan FI. Investigation of Molecular Interactions Mechanism of Pembrolizumab and PD-1. International Journal of Molecular Sciences. 2023 Jun;24(13):10684. Available from: https://doi.org/10.3390/ijms241310684.

[115] Cowles SC, Sheen A, Santollani L, Lutz EA, Lax BM, Palmeri JR, et al. An affinity threshold for maximum efficacy in anti-PD-1 immunotherapy. mAbs. 2022 Aug;14(1). Available from: https://doi.org/10.1080/19420862.2022.2088454.

[116] Ben Saad E, Oroya A, Anto NP, Bachais M, Rudd CE. PD-1 endocytosis unleashes the cytolytic potential of checkpoint blockade in tumor immunity. Cell Reports. 2024 Nov;43(11):114907. Available from: https://doi.org/10.1016/j.celrep.2024.114907.

[117] Zheng Y, Fang YC, Li J. PD-L1 expression levels on tumor cells affect their immunosuppressive activity. Oncology Letters. 2019 Sep. Available from: https://doi.org/10.3892/ol.2019.10903.

[118] Zhu Z, Zhang H, Chen B, Liu X, Zhang S, Zong Z, et al. PD-L1-Mediated Immunosuppression in Glioblastoma Is Associated With the Infiltration and M2-Polarization of Tumor-Associated Macrophages. Frontiers in Immunology. 2020 Nov;11. Available from: https://doi.org/10.3389/fimmu.2020.588552.

[119] Cheng X, Veverka V, Radhakrishnan A, Waters LC, Muskett FW, Morgan SH, et al. Structure and Interactions of the Human Programmed Cell Death 1 Receptor. Journal of Biological Chemistry. 2013 Apr;288(17):11771–11785. Available from: https://doi.org/10.1074/jbc.M112.448126.

[120] Oh SA, Wu DC, Cheung J, Navarro A, Xiong H, Cubas R, et al. PD-L1 expression by dendritic cells is a key regulator of T-cell immunity in cancer. Nature Cancer. 2020 Jun;1(7):681–691. Available from: https://doi.org/10.1038/s43018-020-0075-x.

[121] Snowden TJ, van der Graaf PH, Tindall MJ. Methods of Model Reduction for Large-Scale Biological Systems: A Survey of Current Methods and Trends. Bulletin of Mathematical Biology. 2017 Jun;79(7):1449-86. Available from: https://doi.org/10.1007/s11538-017-0277-2.

[122] Merck. KEYTRUDA (pembrolizumab) injection Label; 2021. https://www.accessdata.fda.gov/drugsatfda_docs/label/2021/125514s096lbl.pdf.

[123] Kazil J, Masad D, Crooks A. In: Utilizing Python for Agent-Based Modeling: The Mesa Framework. Springer International Publishing; 2020. p. 308–317. Available from: https://doi.org/10.1007/978-3-030-61255-9_30.

[124] Sobol' IM. Sensitivity Analysis for Non-Linear Mathematical Models. Math Modeling Comput Exp. 1993;1:407-14.

[125] Cukier RI, Fortuin CM, Shuler KE, Petschek AG, Schaibly JH. Study of the sensitivity of coupled reaction systems to uncertainties in rate coefficients. I Theory. The Journal of Chemical Physics. 1973 Oct;59(8):3873-8. Available from: https://doi.org/10.1063/1.1680571.

[126] Saltelli A, Bolado R. An Alternative Way to Compute Fourier Amplitude Sensitivity Test (FAST). Computational Statistics &amp: Data Analysis. 1998 Feb;26(4):445-60. Available from: https://doi.org/10.1016/s0167-9473(97)00043-1.

[127] Saltelli A, Tarantola S, Chan KPS. A Quantitative Model-Independent Method for Global Sensitivity Analysis of Model Output. Technometrics. 1999;41(1):39-56. Available from: https://doi.org/10.1080/00401706.1999.10485594.

[128] Bellu G, Saccomani MP, Audoly S, D'Angiò L. DAISY: A new software tool to test global identifiability of biological and physiological systems. Computer Methods and Programs in Biomedicine. 2007 Oct;88(1):52–61. Available from: https://doi.org/10.1016/j.cmpb.2007.07.002.

[129] Barua S, Fang P, Sharma A, Fujimoto J, Wistuba I, Rao AUK, et al. Spatial interaction of tumor cells and regulatory T cells correlates with survival in non-small cell lung cancer. Lung Cancer. 2018 Mar;117:73–79. Available from: https://doi.org/10.1016/j.lungcan.2018.01.022.

[130] Maley CC, Koelble K, Natrajan R, Aktipis A, Yuan Y. An ecological measure of immune-cancer colocalization as a prognostic factor for breast cancer. Breast Cancer Research. 2015 Sep;17(1). Available from: https://doi.org/10.1186/s13058-015-0638-4.

[131] Kumbhari A, Egelston CA, Lee PP, Kim PS. Mature Dendritic Cells May Promote High-Avidity Tuning of Vaccine T Cell Responses. Frontiers in Immunology. 2020 Oct;11. Available from: https://doi.org/10.3389/fimmu.2020.584680.

[132] Kumbhari A, Rose D, Lee PP, Kim PS. A minimal model of T cell avidity may identify sub-therapeutic vaccine schedules. Mathematical Biosciences. 2021 Apr;334:108556. Available from: https://doi.org/10.1016/j.mbs.2021.108556.

[133] Chung B, Stuge TB, Murad JP, Beilhack G, Andersen E, Armstrong BD, et al. Antigen-Specific Inhibition of High-Avidity T Cell Target Lysis by Low-Avidity T Cells via Trogocytosis. Cell Reports. 2014 Aug;8(3):871-82. Available from: https://doi.org/10.1016/j.celrep.2014.06.052.

[134] Curtsinger JM, Schmidt CS, Mondino A, Lins DC, Kedl RM, Jenkins MK, et al. Inflammatory Cytokines Provide a Third Signal for Activation of Naive CD4+ and CD8+ T Cells. The Journal of Immunology. 1999 Mar;162(6):3256–3262. Available from: https://doi.org/10.4049/jimmunol.162.6.3256.

[135] Raphael I, Nalawade S, Eagar TN, Forsthuber TG. T cell subsets and their signature cytokines in autoimmune and inflammatory diseases. Cytokine. 2015 Jul;74(1):5–17. Available from: https://doi.org/10.1016/j.cyto.2014.09.011.